ACS Energy LETTERS

http://pubs.acs.org/journal/aelccp

FOCUS REVIEW

Postsynthesis Transformation of Halide Perovskite Nanocrystals

Susmita Paul and Somobrata Acharya*

Cite This: *ACS Energy Lett.* 2022, 7, 2136–2155

Read Online

ACCESS | Metrics & More | Article Recommendations | Supporting Information

ABSTRACT: The high sensitivity of as-synthesized purified perovskite nanocrystals (NCs) to diverse conditions such as solvent polarity, aging, ligand treatment, heat, light, pressure, and humidity affects the surface chemistry. Ligand dynamics (adsorption and desorption) on the surfaces of the NCs plays a key role in the postsynthesis transformation of the morphology and crystallographic phase. Although the ligand destabilization mechanism changes the morphology and crystal structure of the pristine NCs, it also opens up opportunities to obtain interesting morphologies or different crystallographic phases with modified properties. There remain significant challenges in understanding the mechanism of postsynthesis transformation processes. This Focus Review aims to provide a survey of the current state of the postsynthesis transformation of perovskite NCs. The chemistry of controlling the resultant morphology and crystal structure of NCs in the postsynthesis conditions is examined. A more explorative direction for controlling the fundamental properties of the perovskite NCs through postsynthesis transformation is presented.

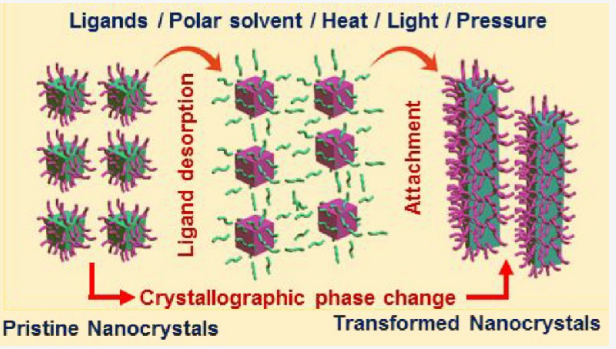

Metal halide perovskite nanocrystals (NCs) with ABX_3 structure, where A is the monovalent cation (A^+), B the divalent cation (B^{2+}), and X the halide ion (X^- = Cl^-, Br^-, I^-),[1,2] are promising candidates for optoelectronic applications because of their tunable band gap, high photoluminescence quantum yield (PLQY), and tunable photoluminescence (PL) through the entire visible region.[3−7] Numerous applications have been demonstrated in solar cells,[8−12] solar concentrators,[13] visible light communications,[14] light-emitting diodes (LEDs),[15−20] photodetectors,[21−23] and photocatalysis[24] using perovskite NCs. Different synthesis procedures have been developed to date to achieve shape-controlled perovskite NCs.[25−32] Among the various synthesis procedures, hot injection (HI), ligand-assisted reprecipitation (LARP) method, and template-based synthesis protocols are the most commonly used techniques to develop perovskite NCs.[33−37] The HI and LARP methods involve use of capping ligands, while the template-based synthesis method requires use of suitable templates to control the resultant shape of the NCs. Capping ligands enable the growth of NCs and actively passivate surface defects. The optical and electronic properties strongly depend on the stoichiometric ratios of the ions in the perovskite structure as well as on the coordination and passivation by ligands and on how the surface is terminated in general.[38−43] Similar to the internal bonding in perovskite NCs, the bonding of ligands to the NC surfaces has a strong ionic character. In polar solvents, the surface-capping ligands are highly dynamic and prone to desorb from the NCs surfaces.[44−47] Additionally, proton exchange between specific coordinating ligands often causes detachment of ligands from the surfaces of the NCs.[47−50] Although these processes present a serious concern to the stability of the pristine perovskite NCs and cause defects, it exposes the NC surfaces for possible postsynthesis morphology and crystallographic phase transformation. Additionally, ligand-exchange procedures also promote desorption of ligands from the NC surfaces by protonation of other ligands. Thus, the introduction of "new" ligands to as-prepared perovskite NCs not only modifies the surface of NCs but also can trigger their postsynthesis transformation.[51−53] Typically, these transformations are accompanied by morphology evolution or crystallographic phase transition with the modified properties of the NCs. Besides this, physical stimuli like light, heat, humidity, or pressure are also able to trigger the chemical reactions to transform the morphologies and phases of the perovskite NCs.

Received: April 16, 2022
Accepted: May 20, 2022
Published: June 1, 2022

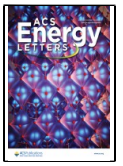

Scheme 1. Transformation Pathways of Pristine Perovskite NCs[a]

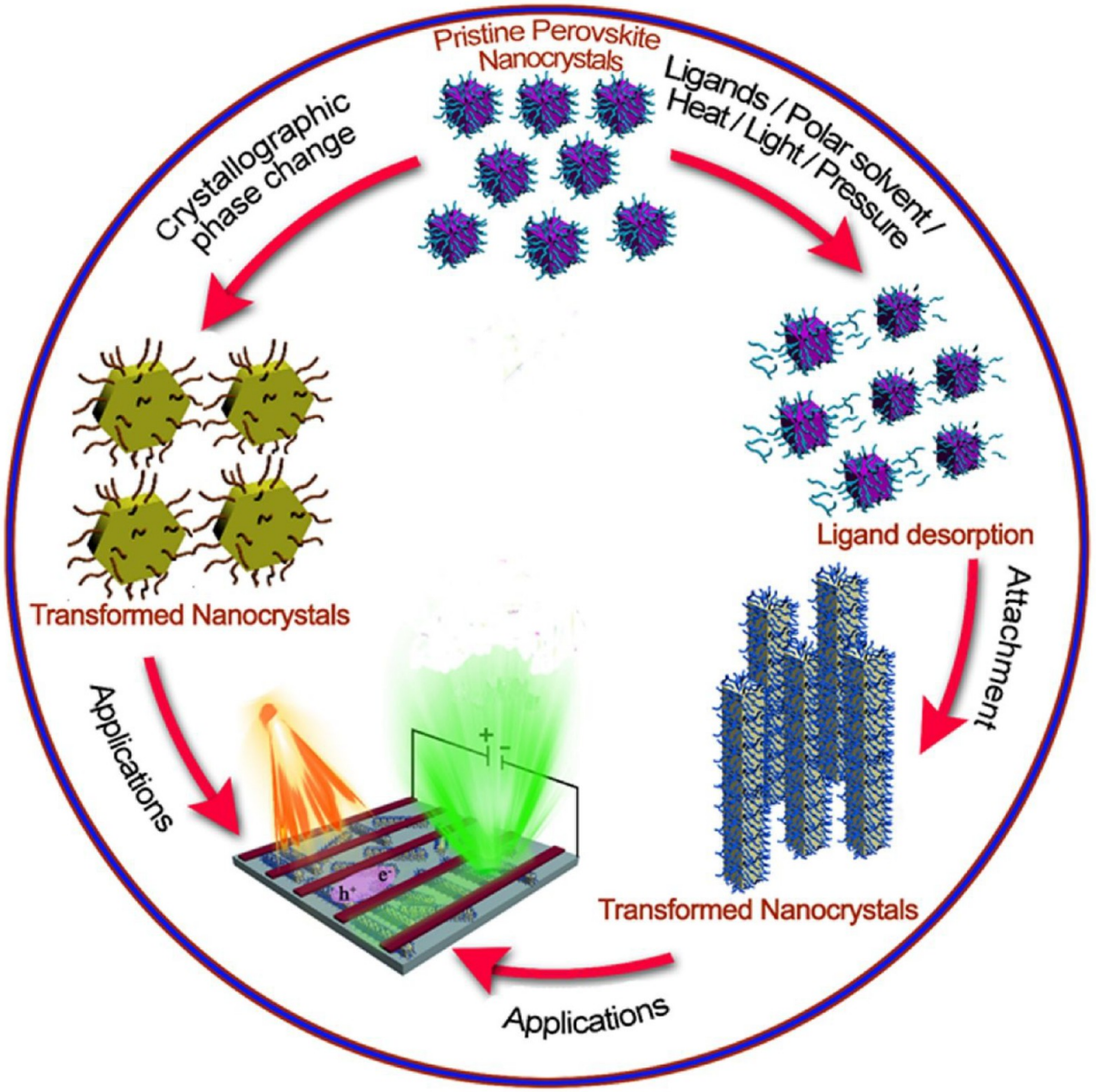

[a]Polar solvent, ligand treatment, heat, light, or pressure can trigger the ligand desorption followed by attachment of the NCs for transformed morphology or the crystallographic phase. The transformed NCs possess modified properties for suitable optoelectronic applications.

In general, postsynthesis transformation involves removal of surface ligands to get rid of steric repulsion followed by interparticle merger or reconstruction of the crystal phase. Because the binding energy of the surface ligands is small and the bonding is highly dynamic,[43−50] light, heat, humidity, or pressure can easily desorb the surface ligands. Hence, postsynthesis chemical or physical treatments are promising methods to transform the morphologies, composition, and structure of the perovskite NCs. Such a change in the morphology or crystal phase also affects the quantum confinement of the NCs and the degree of confinement of the charge carriers to alter the electronic properties.[54−56] Thus, postsynthesis modification of the pristine NCs provides a new way to modify the resultant morphologies, crystallographic phases, and properties suitable for optoelectronic applications.[57−63] However, a review on the postsynthesis transformation of the perovskite NCs is indeed limited to date in comparison to the reviews available on the synthesis and application methods.[64−68] This Focus Review will summarize recent advances in the postsynthesis transformation of the perovskite NCs to achieve morphology or crystallographic phase evolution with modified properties. We will provide a summary of postsynthesis transformation of NCs by means of solvents; ligands; and physical processes such as heat, light, and pressure. The last section will deal with the challenges associated with the postsynthesis transformation of perovskite NCs.

SYNTHESIS OF PEROVSKITE NANOCRYSTALS

The synthesis of various perovskite NCs with tunable morphologies is well-established now. The major approaches for the synthesis of perovskite NCs include HI, LARP, and

https://doi.org/10.1021/acsenergylett.2c00888
ACS Energy Lett. 2022, 7, 2136−2155

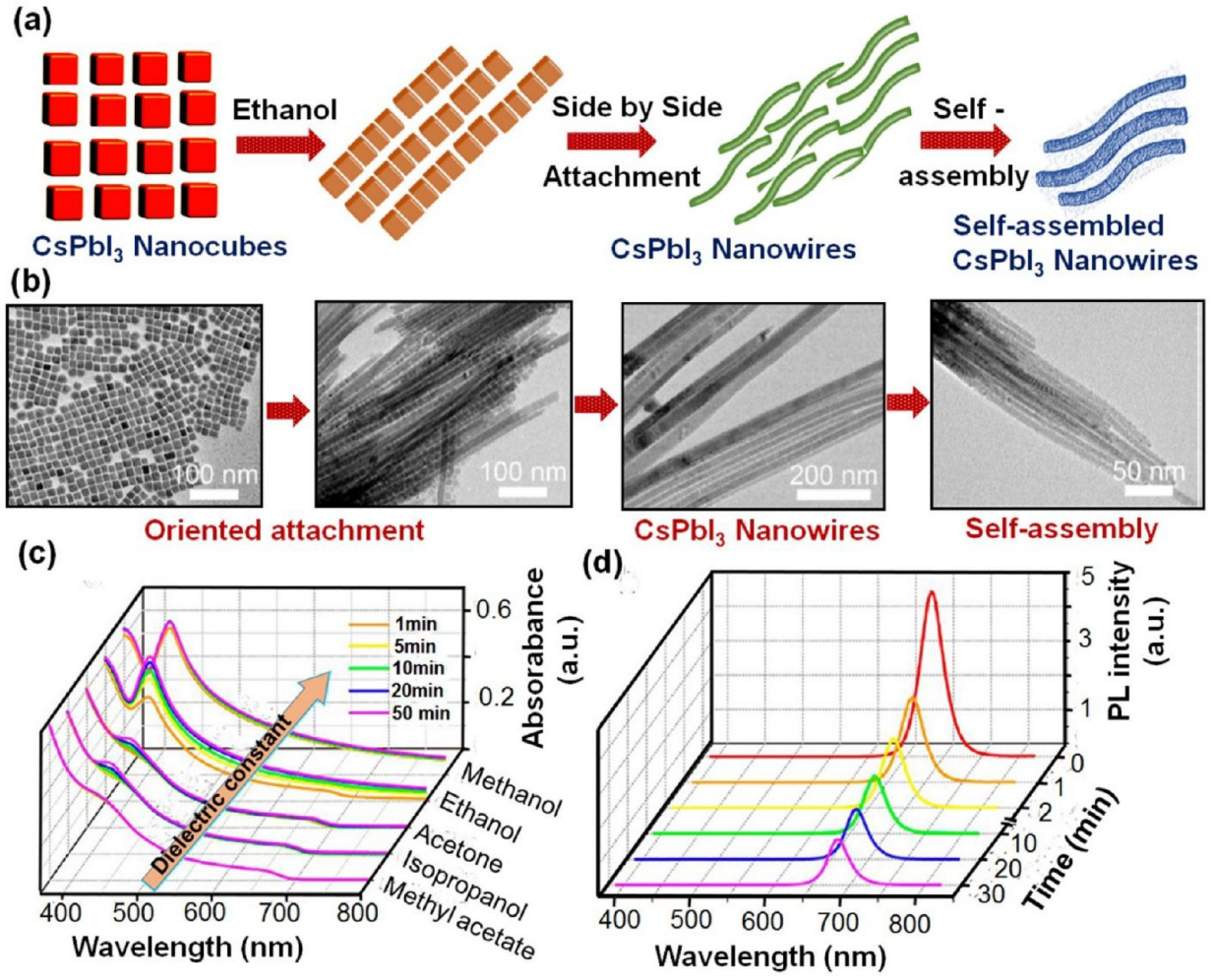

Figure 1. (a) Schematic representation of the polar solvent-induced postsynthesis transformation of $CsPbI_3$ nanocubes into $CsPbI_3$ NWs. (b) TEM images of different stages of $CsPbI_3$ nanocubes to NWs transformation. (c) Time-dependent UV−vis absorption spectra in polar solvents with different dielectric constants. (d) Time-dependent PL spectra of $CsPbI_3$ nanocubes at different time after addition of ethanol. Reproduced with permission from ref 60. Copyright 2018, American Chemical Society.

template-based synthesis.[25−37] The HI and LARP processes involve the use of capping ligands, which dictates the resultant morphology of the NCs. However, the dynamic nature[44−49] of the surface ligands leads to degradation of the morphology of the NCs.[65,69] Hence, the HI and LARP processes often limit the applications of the NCs owing to the stability issues. On the other hand, the use of ligands may be avoided in the template-based synthesis route; however, the resultant morphology of the NCs is solely determined by the templates used in the synthesis.[70,71] The template-based synthesis routes produce opportunities for ligand-free perovskite NCs. The use of templates is advantageous for the stability of the NCs owing to the effective encapsulation. Conversely, the use of templates is disadvantageous for the postsynthesis morphology transformation of the NCs because it requires the removal of the templates.[72]

The most commonly used synthesis route to produce monodispersed NCs is the HI approach.[73−76] The HI process involves the production of homogeneous nuclei via the rapid injection of precursor reagents into a high boiling solvent containing other precursor salts and capping ligands at high temperature followed by homogeneous diffusion-controlled growth.[77,78] The HI method is particularly effective because it offers a high level of control over the size and shape of the resultant high-quality NCs, which can be achieved by varying the temperature of the reaction, concentration of the ligands, and reaction time. The LARP synthesis process holds importance because the formation of NCs takes place within a short time span at room temperature.[79−81] The LARP method involves mixing of the precursor solutions consisting of a polar solvent (good solvent), precursor salts, and capping ligands with a nonpolar solvent (antisolvent) under vigorous stirring at room temperature. Because of the different solubility of salts in polar and nonpolar solvents, the mixing immediately produces a highly supersaturated state and induces fast nucleation and growth of NCs.[79−81] Although, the LARP process leads to quick formation of NCs at room temperature, the rapid nucleation and growth process are disadvantageous in controlling the resultant morphology of the NCs. Several interesting reviews on the HI and LARP synthesis approaches for the perovskite NCs are available.[64,82−89] The scope of the present work is beyond the synthesis of perovskite NCs. This Focus Review will summarize the recent developments in the postsynthesis transformation of perovskite NCs. Because both the HI and LARP methods use capping ligands for surface passivation of the NCs, we will focus on the NCs synthesized

https://doi.org/10.1021/acsenergylett.2c00888
ACS Energy Lett. 2022, 7, 2136−2155

by these methods considering the role of the dynamic nature of the ligands for the postsynthesis transformation.

POSTSYNTHESIS TRANSFORMATION OF PEROVSKITE NANOCRYSTALS

The capping ligands play an integral role in preserving the morphology of perovskite NCs.[90] The strong ionic nature of internal and external bonds leads to rapid formation of perovskite NCs which also cause degradation during the isolation, purification, and storing steps through detachment of the surface ligands.[44−50] In addition, the proton transfer between the oleate species in solution and oleylamine (OLAm) capping ligands can neutralize surface-bound oleylammonium species, which subsequently leave the A-site position on the surface of perovskite NCs.[91] Straight chain aliphatic ligands like OLAm and octylamine with a terminal group of $-NH_2$/NH_3^+ are used to dissolve B-site metal cations in the precursor during the synthesis, which also passivate the surface of the perovskite NCs.[65] Therefore, the selective choice of the surface passivating ligands results in different morphology accompanied by different optoelectronic properties of the perovskite NCs.[51] The postsynthesis morphology transformation also necessitates modification of the NC surfaces. The surface modification of the NCs can be achieved by using polar solvents; by treating the as-synthesized NCs with suitable ligands; or by means of physical processes such as using light, heat, and pressure (Scheme 1). Using postsynthesis techniques, it is also possible to induce a self-assembly of as-prepared NCs in which individual components arrange themselves into an ordered structure (Scheme 1). The postsynthesis transformation of the pristine NCs often triggers interesting morphologies and crystal phase transformation with modified electronic and optical properties, which create opportunities for optoelectronic applications (Scheme 1). In the following section, we will discuss significant routes that reported postsynthesis transformation of the pristine perovskite NCs to a different morphology or crystal phase.

POLAR SOLVENT-INDUCED POSTSYNTHESIS TRANSFORMATION

The strong ionic nature of perovskite NCs makes them interesting defect-tolerant materials; however, it also creates challenges in the stability of the NCs against oxygen, moisture, polar solvent, etc.[44−50,65,69] The large electronegativity difference between the cations and anions originates the inner ionic nature of the perovskite NCs, and the surface bound ligands contribute to the surface ionic nature of the NCs.[92] The commonly used ligands for NC synthesis are OLAm and oleic acid (OA). The oleylammonium cations bind to the surface anions of the NCs. The OA cannot bind to the surface of the perovskite NCs directly but may bind as an ion pair with amine, the actual tightly bound ligand pair being oleylammonium-oleate.[92] Thus, the strong ionic nature of the perovskite NCs leads to the high sensitivity to the polarity of the solvent. The high solubility in polar solvents often leads to poor stability under ambient atmospheric conditions (with variable moisture, heat, light, or pressure). The ligands are more prone to be detached from the surfaces of the NCs upon the use of polar solvents, which results in spontaneous transformation of perovskite NCs during storage.[60,93,94] Precursor−polar solvent interactions indeed play an important role in the postsynthesis transformation of NCs. Aging of the perovskite NCs in such polar solvents can result in a different morphology or crystal phase, which are different from the that of the freshly synthesized NCs. Besides the induced polarity, surface bound ligand desorption in the presence of polar solvent also causes different morphology or crystal phase of the NCs.

The Wan group reported polar-solvent-induced lattice distortion of cubic perovskite (α-phase) $CsPbI_3$ nanocubes into orthorhombic (γ and δ phases) $CsPbI_3$ nanowires (NWs) (Figure 1a).[60] First, $CsPbI_3$ nanocubes were synthesized using PbI_2 and 1-octadecene (ODE) at 120 °C, where OLAm and OA were injected and the reaction temperature was elevated to 170 °C followed by the injection of cesium-oleate. The freshly prepared NCs were perfect nanocubes with uniform size of 14 ± 2 nm, which evolved into NWs with uniform width corresponding to the size of nanocubes upon addition of ethanol (Figure 1b). The pristine cubic $CsPbI_3$ nanocubes did not possess a dipole moment; however, the addition of polar ethanol induced lattice distortion to create a dipole moment via symmetry breaking. Density functional theory (DFT) calculations showed that ethanol preferred to impact onto $CsPbI_3$ instead of alkylamine ligand. The Pb−I−Pb configuration deviated from the original linear states resulting in a "zig-zag" structure while no structural distortion was observed on the whole nanocube. The structure distortion and induced polarization caused reduction of surface energy accompanied by the crystal phase transformation into orthorhombic perovskite phase (γ-phase) and the fall off of alkylamine ligands to reduce the steric repulsion among the $CsPbI_3$ nanocubes. The ethanol-induced polarization of $CsPbI_3$ nanocubes increased over time, and ligands were partially removed from the NC surfaces. The dipole−dipole attraction brought the nanocubes into closer proximity to form single-crystalline NWs with reduced surface energy. Notably, the cubic NC structure distorted slightly to become the orthorhombic γ-$CsPbI_3$ perovskite phase, which finally transformed into the orthorhombic δ-$CsPbI_3$ phase. The cubic α-$CsPbI_3$ and the orthorhombic γ-$CsPbI_3$ phases were both perovskites, as determined by the connectivity of the Pb−I octahedra in the structures, and were related by a mild distortion of the lattice. At a later stage, these distorted NCs fused together forming NWs in the nonperovskite δ-$CsPbI_3$ polymorph that was orthorhombic but was completely different from the initial two structures (α- and γ-phases). The thermodynamically unstable cubic phase of $CsPbI_3$ was stabilized by organic amine ligands. Hence, the addition of polar solvent accompanied with ligand peel-off and lattice fusion led to the phase transformation into the thermodynamically stable orthorhombic δ-phase (Figure 1a,b). The authors observed that the self-assembly and fusion of $CsPbI_3$ nanocubes occurred very quickly compared to the other oriented-attachment and self-assembly in inorganic systems. The NCs showed a color change with time after adding ethanol under visible and UV-light owing to the change in the morphology. Systematic investigations of the kinetics of the self-assembly process revealed that the use of a greater amount of solvent or a solvent with higher polarity induced a more rapid self-assembly and phase transition. For example, methanol (ε = 33.0, where ε is the dielectric constant of the solvent, which is a measure of the solvent polarity) produced NWs in 1 min, while the absorbance change with isopropanol (ε = 18.3) and acetone (ε = 20.7) was much slower (Figure 1c). The resultant NWs' thickness and morphology were controlled by adjusting the concentration of nanocubes in the

https://doi.org/10.1021/acsenergylett.2c00888
ACS Energy Lett. 2022, 7, 2136−2155

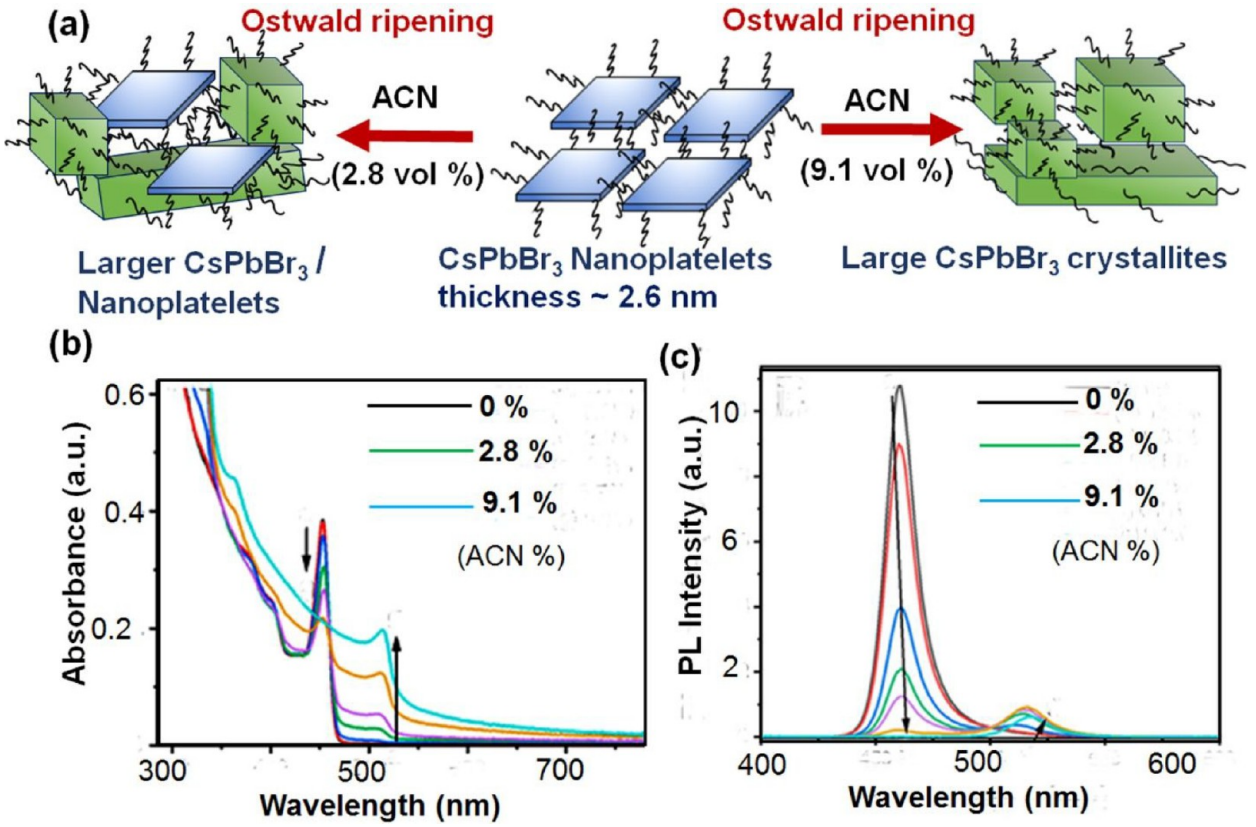

Figure 2. (a) Schematic illustration of polar solvent-induced transformation of $CsPbBr_3$ NPLs into large nanostructures via the Ostwald ripening process. Addition of ACN in small volume (2.8%) resulted in a mixture of NPLs and large crystallites; however, increasing the volume (9.1%) of ACN fully converted the NPLs to larger crystals. Changes in (b) absorbance and (c) PL of $CsPbBr_3$ NPLs in toluene upon increasing the volume fraction of ACN. Reproduced with permission from ref 93. Copyright 2022, American Chemical Society.

solution, polar solvent amount, and assembly process time. Fewer nanocubes, a polar solvent, or short assembly time resulted in thinner NWs. The postsynthesis transformation of the nanocubes was associated with the change in the electronic properties. The kinetics of polar solvent-induced self-assembly by UV−vis absorption spectroscopy revealed a gradual decrease of the absorbance peaks at ∼700 nm of the cubic α-phase $CsPbI_3$ nanocubes and appearance of distinct absorbance peak at 430 nm corresponding to the first absorption band of orthorhombic δ-phase NWs (Figure 1c). The PL spectra indicated a strong red emission at 690 nm for the pristine NCs, which gradually decreased upon self-assembly into NWs (Figure 1d). This study revealed the polar solvent-induced postsynthesis destabilization mechanism of $CsPbI_3$ NCs to induce rapid self-assembly into NWs.

Polar solvent-mediated transformation of the $CsPbBr_3$ perovskite nanoplatelets (NPLs) to larger nanostructures was reported by DuBose et al. (Figure 2a).[93] Transmission electron microscopy (TEM) images of the as-prepared $CsPbBr_3$ NPLs revealed an average thickness of 2.6 ± 0.9 nm corresponding to 4-unit cells. The NPLs were self-assembled in a face-to-face configuration. Interestingly, the addition of mildly polar acetonitrile (ACN) in a small volume (2.8 vol %) led to the formation of a mixture of large crystallites and NPLs. The coexistence of NPLs and larger NCs at intermediate stage indicated a ripening process mimicking the Ostwald ripening mechanism where NPLs were consumed during the formation of larger crystals (Figure 2a). The NPLs fully transformed into larger crystals by increasing the volume fraction of ACN (9.1 vol %). The change in the morphology of NCs upon exposure to ACN changed the optical properties. The pristine $CsPbBr_3$ NPLs exhibited a strong excitonic absorbance peak at 450 nm and a PL peak at 460 nm (Figure 2b,c). Addition of a small volume (5−30 μL) of ACN decreased the PL peak intensity by ∼50%, while at greater ACN volume (>0.85 vol %), a new absorbance peak at 510 nm and a PL peak at 515 nm appeared (Figure 2b,c). These new optical peaks belonged to the larger $CsPbBr_3$ crystals with weaker quantum confinement. The effect of solvent polarity on the morphology transformation by the ripening process was also studied using four other solvents (chlorobenzene, methyl acetate, 2-propanol, and methanol) with different polarity. A small volume of solvent was needed for ripening using more polar 2-propanol and methanol solvents. On the other hand, the less polar methyl acetate and chlorobenzene solvents were required in larger volume for the ripening process. The change in the steady-state optical properties upon exposure to ACN were probed by the excited-state dynamics. A single excitonic bleach band at 460 nm appeared corresponding to the presence of electrons and holes within the $CsPbBr_3$ NPL before addition of ACN. An additional bleached absorption feature centered at 515 nm emerged upon addition of ACN in a small volume, which corresponds to larger $CsPbBr_3$ crystals with weaker quantum confinement. These results highlighted the control of ligand desorption and lowering of the activation energy for ripening using polar solvents for postsynthesis morphology transformation.

https://doi.org/10.1021/acsenergylett.2c00888
ACS Energy Lett. 2022, 7, 2136−2155

The postsynthetic approach provides a fruitful alternative to transform the morphologies and crystallographic phases of the pristine perovskite NCs. The dynamic nature of the coordination between perovskite NC surfaces and the ligands emerged as the key factor for the postsynthesis transformation.

Pradhan et al. reported solvent-assisted spontaneous coalescence of all-inorganic mixed halide $CsPb(Br_xI_{1-x})_3$ ($0 \leq x \leq 1$) perovskite nanocubes into NWs (Figure 3a).[94] $CsPb(Br_xI_{1-x})_3$ perovskite nanocubes were synthesized by a conventional HI method. After synthesis, purified nanocubes were dispersed in toluene and chloroform mixture in 1:1 volume ratio and aged in a refrigerator (4 °C) for several days. TEM images showed the highly monodispersed cubic morphology of the pristine NCs with an average dimension of 9 ± 0.5 nm which was retained up to 7 days of aging (Figure 3b). However, a mixture of nanocubes and NWs was observed after 30 days of aging. The ratio of NWs to nanocubes gradually increased with longer aging, and the conversion of nanocubes to NWs was completed after 60 days of aging. TEM images revealed that the width of the NWs along the entire length remained the same as the width of the nanocubes (Figure 3b). The coexistence of cubic and orthorhombic phases was evidenced when a mixture of nanocubes and NWs was present at the intermediate stages. Finally, a complete transformation into orthorhombic NWs was observed after 60 days of aging, as evidenced from a splitting of the (001) X-ray diffraction (XRD) peak. The XRD patterns showed a crystallographic phase transition from the pure cubic phase (α-phase) of nanocubes to the orthorhombic phase (γ-phase) of the NWs. However, transformation into the orthorhombic nonperovskite δ-phase (the "yellow" phase) was not evidenced. This observation was different from the work of the Wan group,[60] in which the cubic crystallographic phase was finally transformed into the nonperovskite δ-$CsPbI_3$ upon prolonged solvent exposure. TEM images confirmed the growth of the NWs along the ⟨002⟩ direction by the oriented-attachment of nanocubes (Figure 3b). DFT analyses suggested that the dipolar interaction between the adjacent nanocubes led to the oriented-attachment to yield NWs (Figure 3a). The oriented-attachment mechanism depended on the polarity of the solvents and the reactivity of different facets. A complete coalescence of nanocubes into NWs was obtained using a mixed solvent of toluene and chloroform (1:1 by volume) only. The partial removal of ligands from the nanocube surfaces occurred with aging in polar solvent to facilitate the growth of NWs unidirectionally along the ⟨002⟩ direction. The dipole−dipole interaction between the adjacent nanocubes was the major driving force for the solvent-assisted transformation of nanocubes into NWs, similar to the report by the Wan group.[60] However, the transformation of $CsPb(Br_xI_{1-x})_3$ nanocubes was slower compared to the merger of $CsPbI_3$ nanocubes owing to the solvent polarity and aging at reduced

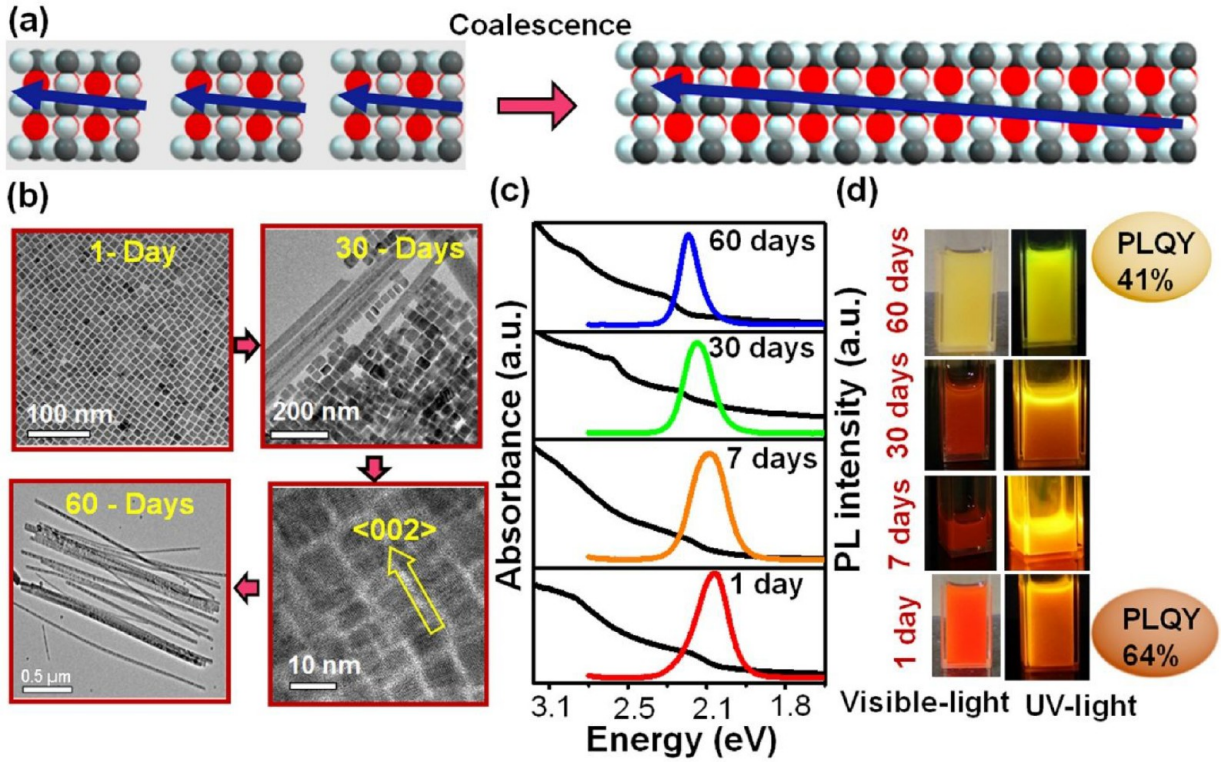

Figure 3. (a) Schematic presentation of the transformation of $CsPb(Br_xI_{1-x})_3$ nanocubes into NWs by dipole−dipole interaction in toluene and chloroform. (b) TEM images at the different stages of nanocube-to-NW transformation. (c) UV−vis absorption and PL spectra of $CsPb(Br_xI_{1-x})_3$ NCs from day 1 to day 60. (d) Photographs of $CsPb(Br_xI_{1-x})_3$ NCs in dispersion at respective days under visible light (left panel) and 365 nm UV-light irradiation (right panel). Reproduced with permission from ref 94. Copyright 2019, American Chemical Society.

https://doi.org/10.1021/acsenergylett.2c00888
ACS Energy Lett. 2022, 7, 2136−2155

temperature (4 °C). Steady-state UV−vis absorption spectra showed a blue shift with different aging time (Figure 3c). Nanocubes showed bright PL with a peak maximum at 2.03 eV at initial stage (1 day) exhibiting absolute PLQY of 64%. However, the PL maximum was blue-shifted from 2.03 to 2.16 eV for the NWs (Figure 3c) upon 60 days of aging. A decrease in the PLQY from 61% to 41% was observed during the morphology transformation from nanocubes to NWs (Figure 3d). The yellow orthorhombic phase (δ-phase) is known to be a nonluminescent nonperovskite phase of the NCs. However, the NWs exhibited PL due to a compositional gradient structure and the perovskite stability in the perovskite orthorhombic γ-phase. The insight mechanism of the PL processes using transient absorption (TA) spectroscopy revealed a faster excited-state decay dynamic with large exciton delocalization length in the one-dimensional (1D) NWs. Strong two-dimensional (2D) quantum confinement owing to the narrow width of the NWs originated the bright PL even after delocalization of charge carriers. These results explored the postsynthesis transformation of the luminescent perovskite nanocubes into luminescent NWs.

LIGAND AND SALT TREATMENT FOR POSTSYNTHESIS TRANSFORMATION

In perovskite NCs the "A-site" cation occupies the corner position, the "B-site" cation remains at the body center, and the "X" anion remains in the face center position. The surface passivating ligands (OLAm, OA, and octylamine) bind to the surface halide ion of the perovskite NCs.[92] However, the bonding between the halide ions and the different ligands depends on the coordinating ability of the ligands. The specific morphology of the perovskite NCs depends on the binding strength of the ligands to the different surface of the NCs.[51,95,96] Besides this, the added surface passivating ligands can also form strong complexes with the salts of A and/or B-site cations which prevents the cations from taking part in the reaction and can also lead to different morphology or crystal phase. Hence, postsynthesis treatment of as-synthesized NCs with different amines, acids, or salts produces different chemical environment for the NCs for the transformation. The reconstruction process has important implications for the thermodynamics and energetics of the perovskite NCs. However, a proper understanding of the complex reconstruction processes occurring at the surfaces is still limited.[61,96,97]

Palazon et al. reported on the postsynthesis transformation of three-dimensional (3D) $CsPbBr_3$ nanocubes to zero-dimensional (0D) Cs_4PbBr_6 NCs by adding amine at room temperature.[61] Monodispersed $CsPbBr_3$ nanocubes (~8 nm) were synthesized using the HI method, which were later treated with tetramethylethylenediamine (TMEDA) for the transformation to rhombohedral Cs_4PbBr_6 NCs. A white precipitate consisting of rhombohedral (in projection view) shaped polydisperse Cs_4PbBr_6 NCs with sizes of ~50 nm was observed upon exposing the toluene dispersion of $CsPbBr_3$ nanocubes to TMEDA for a few minutes. The transformation was reflected in the optical UV−vis and PL spectra. The UV−vis spectra measured immediately after the transformation were drastically different from those of the starting nanocubes. The exciton absorbance peak at 500 nm typical of the 3D phase $CsPbBr_3$ disappeared, and a sharp characteristic absorbance peak at 317 nm of the 0D phase Cs_4PbBr_6 appeared. The transformation upon amine treatment was attributed to the strong coordination of the diamino group with Pb^{2+} ions, which led to a rapid transformation from 3D to 0D NCs. Extraction of $PbBr_2$ took place from the 3D $CsPbX_3$ NCs upon addition of amines, which led to the dissolution of the starting NCs to form the 0D Cs_4PbBr_6 NCs. Such transformation followed $4CsPbBr_3 \rightarrow Cs_4PbBr_6 + 3PbBr_2$ reaction pathways, where the excess $PbBr_2$ formed stable complexes with the added TMEDA. A different amine, such as OLAm, butylamine, etc., also resulted in different morphologies of the NCs. The treatment of butylamine vapor on the thin film of $CsPbBr_3$ NCs prepared on a TEM grid also resulted in 3D-to-0D phase transformation of the NCs. Upon exposure to the amine, the starting $CsPbBr_3$ nanocubes with an orthorhombic crystal structure transformed into rounded Cs_4PbBr_6 NCs, and the transformation process was reversible because annealing of the TEM grid at 100 °C resulted in orthorhombic 3D perovskite structures. These results demonstrated a facile method of postsynthesis transformation of the shape and structure and consequently the modification of optical properties of cesium lead halide NCs in solution and in solid films by the addition of different amines at room temperature. The tuned optical properties associated with the phase change may be useful for suitable optoelectronic applications.

Although the postsynthetic transformation introduces opportunities to change the morphologies and properties of the as-synthesized perovskite NCs, there are several open issues that require attention. It is important to understand the growth kinetics, assembly mechanisms, and surface ligand chemistry during the postsynthesis transformation process.

Conversely, the Cs_4PbBr_6 NCs were converted into $CsPbBr_3$ NCs by the reaction with an excess of $PbBr_2$ with preservation of size distributions. The Cs_4PbBr_6 NCs were prepared by using an excess of cesium-oleate and lowering the reaction temperature.[62] The reaction resulted in nearly monodisperse Cs_4PbBr_6 NCs ranging from 9 to 37 nm. The NCs exhibited a strong and narrow optical absorption band at 314 nm regardless of the NC sizes. The sizes of the NCs do not contribute to the electronic properties because the $[PbX_6]^{4-}$ octahedra in the Cs_4PbBr_6 NCs were completely decoupled and the excitons were localized in $[PbX_6]^{4-}$ octahedra. The resultant Cs_4PbBr_6 NCs were exposed to a solution of $PbBr_2$ dissolved in OLAm, OA, and toluene to obtain $CsPbBr_3$ NCs. This process resulted in the change of crystallographic phase, which transforms the morphology of the NCs from a spherical/hexagonal shape to cubic NCs retaining the overall size. The formation of the $CsPbBr_3$ phase was associated with a large red shift of the absorption band from 314 to 510 nm and the emergence of a strong green PL in the 511−522 nm region depending on the sizes of the NCs. This postsynthesis transformation is yet more proof of the change in crystal structure to tune the electronic properties of perovskite NCs.

The Manna group also reported transformation of Cs_4PbBr_6 NCs to $CsPbBr_3$ NCs induced by copolymer poly(maleic anhydride-alt-1-octadecene) (PMAO).[98] First, Cs_4PbBr_6 NCs

https://doi.org/10.1021/acsenergylett.2c00888
ACS Energy Lett. 2022, 7, 2136−2155

were synthesized via the HI method. Rhombohedral shape Cs_4PbBr_6 NCs with size ~10−16 nm showed an absorbance peak at 314 nm. The postsynthetic transformation was carried out by treating the toluene solution of pristine NCs with PMAO at mild heating conditions. The amount of PMAO determined the partial or complete transformation of the NCs. Upon mixing, PMAO reacted with OLAm available in the NC solution forming polysuccinamic acid which destabilized the NC surfaces by displacing both the amine and oleate ligands to form $CsPbBr_3$ NCs. Interestingly, the Cs_4PbBr_6 NCs synthesized with trioctylphophine oxide and OA were unreactive toward PMAO. Intermediate stages of the reaction showed heterostructures with distinct interfaces between Cs_4PbBr_6 and $CsPbBr_3$ species. The fully transformed $CsPbBr_3$ NCs showed enhanced stability compared to the pristine NCs owing to the efficient binding by polysuccinamic acid. Palazon et al. reported a similar type of postsynthesis transformation of Cs_4PbBr_6 NCs to $CsPbBr_3$ NCs by treatment with Prussian blue $[Fe(III)_4[Fe(II)(CN)_6]_3]$.[99] The transformation reaction was carried out by adding $Fe(III)_4[Fe(II)(CN)_6]_3$ to a toluene solution of Cs_4PbBr_6 NCs for 1 day at room temperature. The transformation process was accompanied by the disappearance of a sharp absorbance peak at 314 nm of the pristine Cs_4PbBr_6 NCs followed by the appearance of new absorbance and PL characteristic peaks of $CsPbBr_3$ NCs at 500 and 515 nm, respectively. TEM images showed a contraction of size of the transformed NCs (~6.3 nm) compared to the pristine NCs (~9.8 nm), suggesting that the transformation was accompanied by etching of the NCs. They have also applied this technique for the transformation of Cs_4PbI_6 NCs into $CsPbI_3$ NCs. However, the attempt to transform the NCs by thermal annealing of pristine Cs_4PbBr_6 NCs resulted in incomplete transformation to $CsPbBr_3$ NCs in the temperature range of 150−350 °C due to desorption of residual toluene and partial extraction of Cs^+ and Br^- ions, which formed complexes with the residual long-chain ligands. Further increase of the temperature to 400 °C brought back the pristine Cs_4PbBr_6 NCs only.

The reversible morphology transformation of the $CsPbBr_3$ NPLs to Cs_4PbBr_6 NCs was demonstrated by Zhai et al.[100] $CsPbBr_3$ NPLs were converted to Cs_4PbBr_6 NCs by increasing the amount of cesium-oleate precursor, and the reversible transformation of Cs_4PbBr_6 NCs to $CsPbBr_3$ NPLs was achieved by adding a certain amount of $PbBr_2$−precursor ($PbBr_2$ dissolved in a mixture of OLAm, OA, and ODE; Figure S1 of the Supporting Information). Cubic phase $CsPbBr_3$ NPLs were synthesized using $PbBr_2$ and cesium-oleate precursors by a solvothermal method. $CsPbBr_3$ NPLs showed tunable absorbance peak positions ranging from 446 to 460 nm and PL peak from 453 to 465 nm with an increase of reaction time. Rhombohedral Cs_4PbBr_6 phase NCs were achieved by gradually increasing the amount of cesium-oleate precursor. Optical studies indicated that the transformed Cs_4PbBr_6 NCs exhibit different absorbance and PL peaks compared with initial $CsPbBr_3$ NPLs. Optical spectroscopy revealed a characteristic absorbance peak at ~314 nm of Cs_4PbBr_6 NCs. A weak PL was observed from Cs_4PbBr_6 NCs corresponding to the minor $CsPbBr_3$ impurities mixed in the nonemitting Cs_4PbBr_6 product, although no trace of $CsPbBr_3$ was found in the XRD patterns (Figure S1c). Alternatively, postsynthesis chemical transformation from Cs_4PbBr_6 NCs to $CsPbBr_3$ NPLs was achieved by reacting a certain amount of $PbBr_2$−precursor in the presence of the ligands. The characteristic optical peaks of $CsPbBr_3$ NPLs reappeared after the reversible transformation reaction (Figure S1c). The reversible transformation process was associated with the crystal phase transformation between cubic $CsPbBr_3$ and rhombohedral Cs_4PbBr_6. The postsynthesis route demonstrated successful control over the morphology, crystallographic phase, and composition of cesium lead halide NCs.

Yang et al. reported postsynthesis transformation of spherical 0D Cs_4PbBr_6 NCs into $CsPbBr_3$ NWs using different combinations of ligands (Figure S2).[101] First, Cs_4PbBr_6 NCs were prepared by the HI technique. TEM images revealed the spherical morphology of Cs_4PbBr_6 NCs with average diameter of 12.1 ± 1.0 nm (Figure S2a). The Cs_4PbBr_6 NCs showed an absorbance peak centered at 426 nm; however, no PL peak was observed. For the transformation to $CsPbBr_3$ NWs from the Cs_4PbBr_6 NCs, the postsynthetic treatment was carried out by mixing a hexane solution of spherical Cs_4PbBr_6 NCs with solid $PbBr_2$ precursors and two short alkyl chain ligands (hexanoic acid and octylamine) along with OA. TEM images of the transformed NCs revealed thin NWs of 2.5 ± 0.6 nm width and length >10 μm (Figure S2b). UV−vis absorption spectra showed a gradual appearance of a new absorbance peak at 426 nm, and PL spectra showed a strong blue PL peak centered at 432 nm corresponding to the excitonic emission of the NWs with strong quantum confinement (Figure S2c). The transformation mechanism was investigated by TEM images for the samples captured during the transformation reaction. TEM images showed coexistence of both the pristine spherical Cs_4PbBr_6 NCs and the newly formed $CsPbBr_3$ NWs, suggesting a dissolve-then-reform mechanism of the transformation reaction. Similarly for the synthesis of $CsPbBr_3$ nanocubes, the authors used hexane solution of spherical Cs_4PbBr_6 NCs along with solid $PbBr_2$-precursors with trioctylamine (Figure S2d). The resulting NCs showed a nanocube morphology with a characteristic PL peak at 515 nm (Figure S2e). They speculated that $PbBr_2$-ligand intermediates played a key role in determining the NW or nanocube shape of the transformed NCs. Thus, various $PbBr_2$-ligand intermediates were prepared by reacting $PbBr_2$ solid precursor with different ligand combinations (hexanoic acid, octylamine, and trioctylamine) in toluene. The chain type amine ligands produced anisotropic lamellar $PbBr_2$-ligand structures, whereas bulky branched trioctylamine ligand led to the formation of isotropic $PbBr_2$-ligand intermediates. Interestingly, the anisotropic lamellar $PbBr_2$-ligand intermediates resulted in formation of NWs, and other isotropic ligand intermediates produced nanocubes. The spectral and morphological features of the NWs obtained via postsynthesis transformation process showed a close resemblance with the directly synthesized NWs.[102] The formation of ultrathin NWs is a challenging task that requires delicate control of nucleation and growth processes in the direct synthesis route. This postsynthetic technique offered a new way to obtain quantum-confined ultrathin perovskite NWs, in addition to the nanocubes.

Core−shell NCs exhibit improved PL owing to the reduced surface defects imposed by the shell. Jia et al. reported on the postsynthesis fabrication of the Cs_4PbX_6 shell on the core of $CsPbX_3$ NCs. They have synthesized the $CsPbX_3/Cs_4PbX_6$ core−shell NCs by adopting a seeded growth approach.[103] First, the core $CsPbBr_3$ NCs were prepared by a conventional HI approach. Then, the shell coating was developed by postsynthetic treatment with a halide source (zinc bromide) and rapidly injecting cesium-oleate into the pristine $CsPbBr_3$

https://doi.org/10.1021/acsenergylett.2c00888
ACS Energy Lett. 2022, 7, 2136−2155

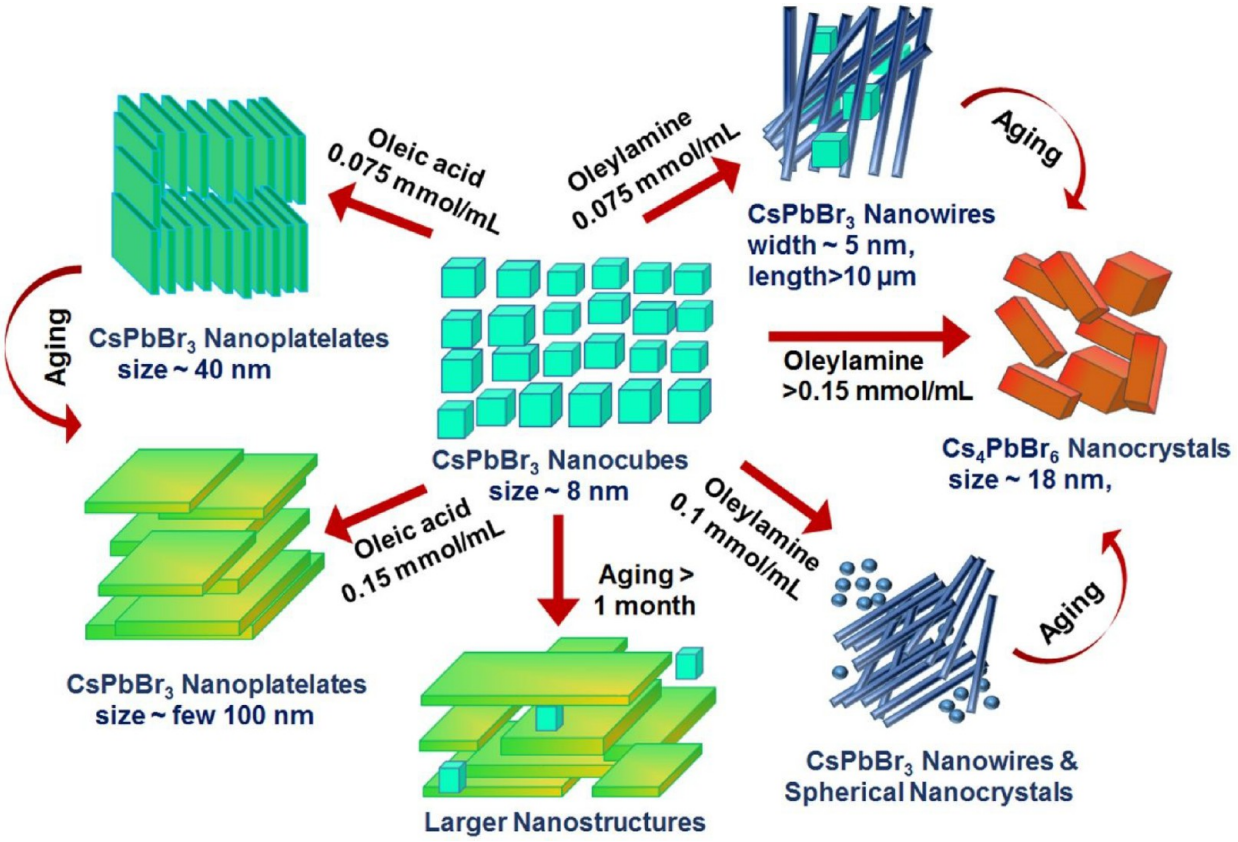

Figure 4. Schematics of morphology transformation of $CsPbBr_3$ nanocubes upon ligand addition and aging. Addition of variable amount of OLAm promotes the transformation of nanocubes into 1D NWs and rhombohedral nanostructures, whereas the addition of OA in different volumes resulted in 2D anisotropic NPLs. Reproduced with permission from ref 107. Copyright 2019, Tsinghua University Press and Springer-Verlag GmbH Germany, part of Springer Nature.

NCs. Similarly, other halide $CsPbX_3/Cs_4PbX_6$ (X = Cl, I) core−shell NCs were prepared. The amount of halide source determined the thickness of the shell. The core−shell NCs showed improved PLQY of 12% compared to the pristine NCs because the Cs_4PbBr_6 shell with a large band gap helped to confine the excitons in the core as well as reduced the surface defect states. The core−shell NCs showed improved PL stability for a number of days. This work demonstrated the postsynthesis chemical modification to improve the stability of the pristine NCs.

Postsynthesis surface trap removal of $CsPbX_3$ (X= Cl, Br, I) NCs was reported by the Xia group.[104] The TEM images of pristine NCs showed "black dots" on the surface due to PbX_2 formation by the decomposition of $CsPbX_3$ NCs. The pristine NCs were treated with ZnX_2 in a mixture of hexane and OLAm, which led to the disappearance of the "black dots" as the ZnX_2 treatment led to healing of halogen defects (Figure S3a). The halogen of ZnX_2 occupied the halide vacancy, which prevented the decomposition of $CsPbX_3$ NCs. The ZnX_2-treated NCs showed considerable improvement of the PLQY because of the reduced surface defects. They have fabricated phosphor-conversion white light-emitting diodes (pc-WLED) with the $ZnBr_2$-treated $CsPbBr_3$ (Figure S3b−d) utilizing improved PLQY.

Ji et al. reported on the anion exchange-triggered morphology transformation of $CsPbBr_3$ NWs.[105] $CsPbBr_3$ NWs were synthesized by oriented-attachment of $CsPbBr_3$ NCs of ∼3.0 nm diameter. The absorbance peak shifted to a higher wavelength with the morphological evolution from NCs to NWs. These NWs were subjected to anion exchange reactions by treatment with tetrabutylammonium chloride (TBA-Cl) and tetrabutylammonium iodide (TBA-I). Typically, $CsPbBr_3$ NWs were mixed with TBA-Cl or TBA-I and OLAm in argon (Ar) atmosphere for the anion exchange reactions. The chlorine exchange resulted in spherical NCs of ∼5 nm size, whereas iodine exchange resulted in hexagonal NCs of ∼20 nm size. The optical properties of the $CsPbBr_3$ NWs before and after the anion exchange were different. The PL peak at 457 nm for $CsPbBr_3$ NWs was red-shifted with increasing iodide content and blue-shifted as the chloride content was increased.

Because of the ionic nature of the perovskite NCs, the halide ions in the perovskite NCs undergo rapid exchange in the presence of other halide ions. However, the anion exchange can be prevented by postsynthesis coating of the pristine NCs. Ravi et al. reported postsynthetic $PbSO_4$-oleate capping of $CsPbBr_3$ and $CsPbI_3$ NCs.[106] The pristine NCs were synthesized by the HI method. A pristine NC solution in hexane was added to the $PbSO_4$-oleate cluster prepared in chloroform to put coating on the pristine NCs. TEM images showed the linear alignment of capped NCs on the TEM grid. The capping layer kept well-dispersed NCs with minimal interparticle interactions. The absorbance and PL features of the NCs did not alter after capping with $PbSO_4$-oleate, suggesting that the capping layer did not contribute to the band structure of the pristine NCs. When the pristine $CsPbBr_3$ and $CsPbI_3$ NCs were mixed together, the absorbance and PL peaks of the pristine NCs merged into a single peak owing to

https://doi.org/10.1021/acsenergylett.2c00888
ACS Energy Lett. 2022, 7, 2136−2155

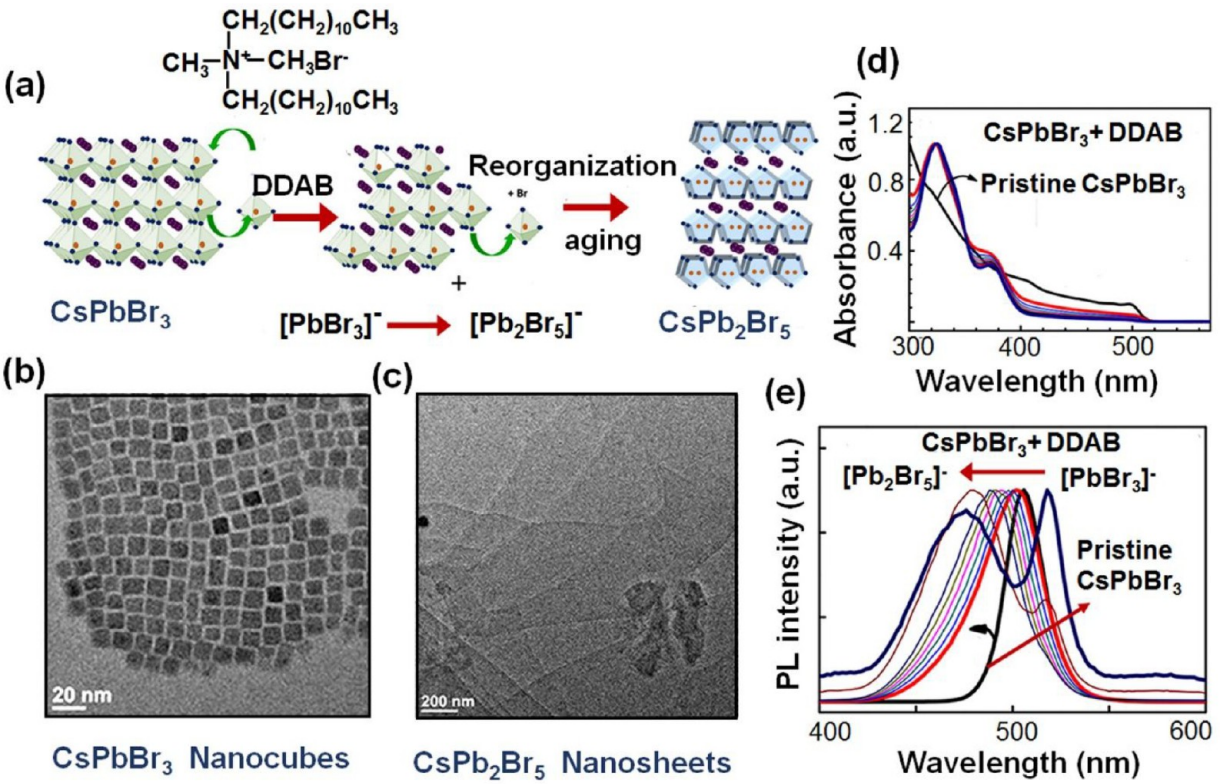

Figure 5. (a) Schematic representation of ligand-assisted exfoliation and transformation of cubic $CsPbBr_3$ NCs to tetragonal $CsPb_2Br_5$ NSs. TEM images of (b) $CsPbBr_3$ NCs and (c) $CsPb_2Br_5$ NSs. (d) Absorption spectra with the reaction with DDAB with aging. (e) PL spectra with the reaction with DDAB with aging. Reproduced with permission from ref 109. Copyright 2018, American Chemical Society.

the anion exchange. When the capped NCs were mixed together, the absorption spectra did not show any noticeable shift in the peaks. However, the PL peak showed a small shift owing to the halide ion exchange between poorly capped or uncapped NCs or from deterioration of the $PbSO_4$-oleate capping layer under stirring. This work demonstrated that the $PbSO_4$-oleate capping offered a new approach to prevent the anion exchange of cesium lead halide NCs while retaining the optical properties.

Fanizza et al. reported on the postsynthesis morphology evolution of $CsPbBr_3$ NCs under the influence of aliphatic carboxylic acids (OA) and alkyl amines (OLAm) (Figure 4).[107] $CsPbBr_3$ NCs are synthesized by using the HI approach. The TEM images revealed a cubic morphology of the NCs with average lateral size of ∼8 nm. The NCs showed a characteristic narrow and intense PL peak at 505 nm. Aging-induced morphological transformation of these nanocubes yielded larger polydispersed nanostructures upon prolonged (more than one month) air/moisture and light exposure (Figure 4). This transformation of morphology was reflected in the PL spectrum consisting of two peaks at 505 and 519 nm corresponding to the residual 8 nm sized nanocubes and larger nanostructures, instead of one peak of nanocubes. Postsynthesis addition of OLAm (0.075 mmol/mL) to the solution of $CsPbBr_3$ NCs induced the morphology transformation of the freshly prepared 3D nanocubes into NWs of 5 nm width and micrometer length. The length of the NWs increased upon increasing the amount of OLAm (0.1 mmol/mL), retaining the same 5 nm width, although spherical NCs of nearly 17 nm diameter were also evidenced (Figure 4). Further increase of OLAm (>0.15 mmol/mL) led to the formation of rhombohedral shaped nanostructures with a lateral size of nearly 18 nm (Figure 4). The absorbance peak of the NWs did not show appreciable change compared to the pristine NCs; however, the PL spectrum displayed significant band broadening and a marked quenching with respect to the pristine NCs. Notably, $CsPbBr_3$ NWs of comparable dimension synthesized directly by the HI method showed bright blue emission.[102,108] Bright blue emission was also evidenced from the $CsPbBr_3$ NWs obtained from the postsynthesis transformation of nonemitting Cs_4PbBr_6 NCs.[101] Similar morphological evolution was also achieved by adding a shorter alkyl chain amine, octylamine. Very thin NWs were evidenced upon addition of 0.08 M octylamine, and rhombohedral structures appeared at increased octylamine concentration (0.2 M). While alkyl amine addition promoted the transformation of nanocubes into 1D NWs and rhombohedral nanostructures, the addition of OA (nonanoic acid are also tested) to the solution of the as-prepared 3D $CsPbBr_3$ nanocubes resulted in 2D anisotropic NPLs. The formation of NPLs was independent of the amount of added OA. NPLs of 4 nm thickness and lateral size up to nearly 40 nm were evidenced upon addition of OA in a smaller amount (0.075 mmol/mL). Larger NPLs with lateral size of a few hundred nanometers were obtained upon increasing the amount of OA (0.15 mmol/mL) (Figure 4). The smaller NPLs turned into polydisperse NPLs with micrometer size upon longer aging. The absorption spectrum of OA-treated samples showed an exciton transition signal blue-shifted to 485 nm compared to the as-prepared 3D $CsPbBr_3$ nanocubes. The PL spectrum exhibited a main band at 503 nm corresponding to residual nanocubes and a blue-shifted shoulder at nearly 480 nm attributed to NPLs with thickness smaller than the Bohr

https://doi.org/10.1021/acsenergylett.2c00888
ACS Energy Lett. 2022, 7, 2136−2155

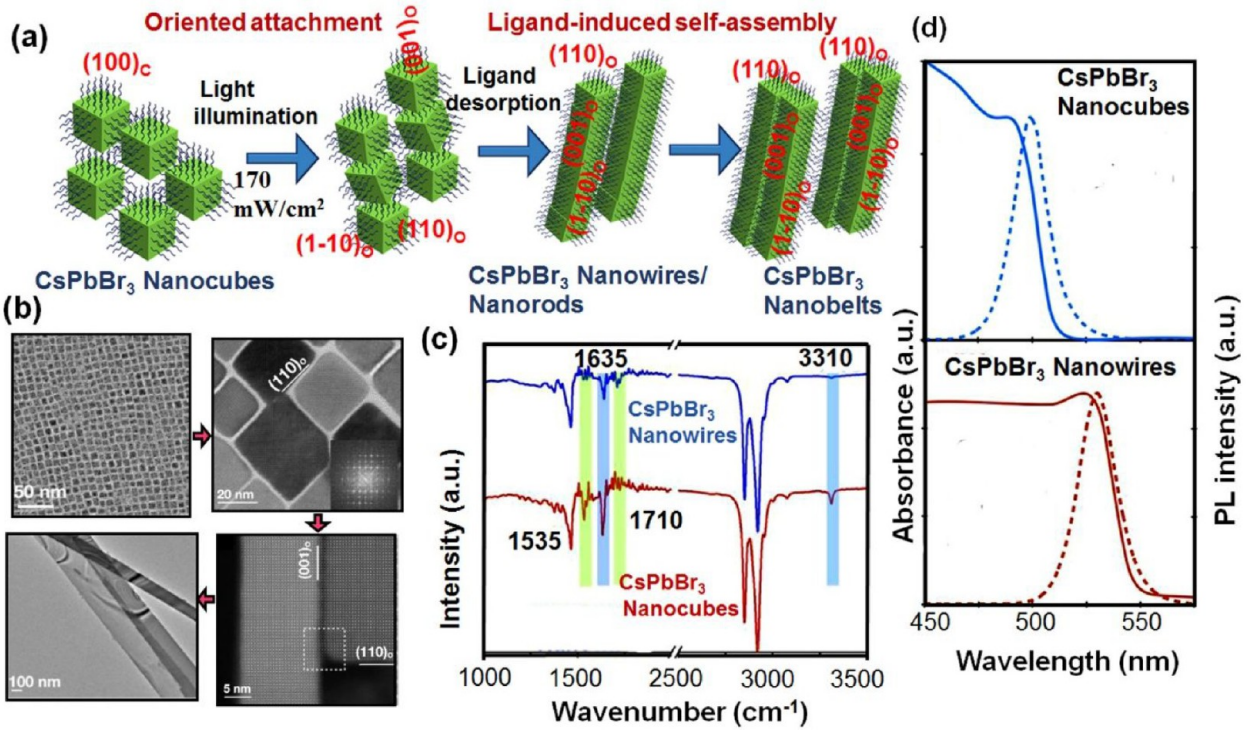

Figure 6. (a) Illustration of morphology evolution of $CsPbBr_3$ nanocubes to NWs/NRs and nanobelts driven by light illumination (1.7 suns, 170 mW/cm^2). Light illumination induced the ligand desorption from the surface of the NCs to promote the oriented attachment of the nanocubes into NWs/NRs/nanobelts. (b) TEM images at different stages of morphology transformation process. (c) FTIR spectra of nanocubes and NWs showing spectral shift upon ligand desorption. (d) UV−vis and PL spectra showing red-shift of the peak positions of NWs compared to the nanocubes. Reproduced with permission from ref 121. Copyright 2019, American Chemical Society.

diameter. This work demonstrated an intriguing approach for postsynthesis morphology evolution of $CsPbBr_3$ nanocubes upon OLAm and OA treatment, in addition to the dilution and aging.

The Kamat group reported on the postsynthesis transformation of $CsPbBr_3$ nanocubes into 2D $CsPb_2Br_5$ nanosheets (NSs) by using dodecyldimethylammonium bromide (DDAB) (Figure 5a).[109] Pristine $CsPbBr_3$ nanocubes were synthesized by the HI technique and treated with DDAB for the postsynthesis transformation. TEM images of the pristine $CsPbBr_3$ showed monodispersed nanocubes with size of 7 ± 2 nm, which transformed to NSs with micrometer size upon DDAB treatment (Figure 5b, c). The $CsPbBr_3$ NCs exhibited an absorbance shoulder at ∼500 nm. On addition of DDAB, a marked change was observed with decreased absorbance in the 400−520 nm region as a result of the first step of ligand exchange. The increase of the absorbance at 320 nm corresponded to the $[PbBr_3]^-$ complex formation and represented the initial chemical transformation induced by DDAB followed by appearance of a new peak at ∼340 nm corresponding to the stable $[Pb_2Br_5]^-$ complex (Figure 5d). A blue-shift of the PL peak was observed with decrease in the PLQY from 70% to 4% (Figure 5e). The transformation of the $[PbBr_3]^-$ complex into the $[Pb_2Br_5]^-$ complex favored the formation of a sheet morphology. The effect of dodecyl amine (DDA) was also tested; however, addition of DDA did not permit morphological transformation. These observations implied that the selection of the ammonium cation was important for inducing exfoliation of the perovskite lattice. This work demonstrated the importance of the selection of the ligand to transform the postsynthesis morphology of perovskite structures.

Similar to the lead halide perovskite, morphology transformation and crystallographic phase change also modify the properties of lead-free halide perovskites. The Chen group reported the transformation of 0D Cs_3BiX_6 (X= Cl, Br) NCs into 2D $Cs_3Bi_2X_9$ NCs via postsynthesis modification with BiX_3 solution.[110] Pristine Cs_3BiX_6 NCs were synthesized by the HI method. Cubic Cs_3BiCl_6 (9.8 ± 1.3 nm) and Cs_3BiBr_6 (10.9 ± 1.5 nm) NCs showed absorbance peaks at 332 and 380 nm, respectively. For the postsynthesis transformation, toluene solution of Cs_3BiX_6 NCs was treated with a mixture of BiX_3, OLAm, and OA. The transformation process occurred via the disappearance of the original absorbance peaks followed by formation of new absorbance peaks at 370 and 430 nm for the $Cs_3Bi_2Cl_9$ and $Cs_3Bi_2Br_9$ NCs, respectively. Though this postsynthesis transformation led to a phase change from 0D to 2D, the transformed NCs retained a cubic morphology similar to that of the pristine NCs. In another work, the same group reported on the formation of 3D Cs_2AgBiX_6 double-perovskite NCs from 0D Cs_3BiX_6 NCs (X= Cl, Br) and 2D $Cs_4MnBi_2Cl_{12}$, $Cs_4CdBi_2Cl_{12}$ layered double-perovskite NCs from 0D Cs_3BiCl_6 NCs via postsynthetic treatment with metal salts.[111] Postsynthetic transformation reactions were carried out by adding an ACN solution of silver nitrate ($AgNO_3$) to the hexane solution of Cs_3BiX_6 NCs at 50 °C. Ag-doped 0D Cs_3BiX_6 NCs were formed after the addition of Ag^+ cations with Ag^+ ions occupying the Cs^+ sites. Partial phase transition occurred from the 0D Cs_3BiX_6 phase to the double-perovskite phase where both $[AgX_6]^{5-}$ and $[CsX_6]^{5-}$ octahedra units were formed by corner sharing of the X^- ions with the $[BiX_6]^{3-}$

https://doi.org/10.1021/acsenergylett.2c00888
ACS Energy Lett. 2022, 7, 2136−2155

octahedra. Increase of Ag^+ concentration led to the intermediate $Cs_2(Ag_xCs_{1-x})BiX_6$ alloyed double-perovskite crystal motif. Further increase of Ag^+ concentration formed the Cs_2AgBiX_6 double-perovskite NCs. TEM images revealed the unchanged NC morphology of the transformed NCs similar to the pristine NCs, as observed in the previous case.[110] In a similar way, 2D $Cs_4MnBi_2Cl_{12}$ and $Cs_4CdBi_2Cl_{12}$ layered double-perovskite NCs were synthesized using postsynthesis treatment of Cs_3BiCl_6 NCs with $MnCl_2$ and $CdCl_2$ salts. Unlike the previous reports, these transformed NCs showed a change in the morphology owing to the distortion of $[BiCl_6]^{3-}$ octahedra of the pristine NCs. These postsynthesis procedures avoided the use of multiple components and possible reaction side-products for the synthesis of double perovskites.

PHYSICAL PROCESSES FOR POSTSYNTHESIS TRANSFORMATION

Light-induced synthesis and morphology transformation have gained interest as promising alternative routes to realize new types of materials structures. Light can be used to stimulate the synthesis of light-responsive materials. Interestingly, halide perovskite NCs tend to respond to light. Light has significant effect on the nucleation and growth, phase transition, structural dynamics, ion migration, conductivity, etc.[112−115] Interestingly, surface ligands are also sensitive to the light, which causes light-induced desorption of ligands from the perovskite NC surfaces followed by transformation of the morphology or crystallographic phase of the NCs. Besides the light, heat is the other important physical parameter to transform the pristine perovskite NCs. The common type of defect present in perovskite NCs is Frenkel defects originating from charge separation at the surfaces of the NCs. The halide vacancies are the dominant diffusing defect because of the lower formation energy and low diffusion barriers. At the same time, the interstitial halide ions tend to go to the surfaces to reduce the corresponding elastic energy. Predominantly, this causes the formation of defects near the surfaces where the halide ions can easily move to the surface, leaving halide vacancies in the surface layer.[116] Hence, heat can affect the diffusion rate of the ions, which governs the particular morphology and crystallographic phase of perovskite NCs by overcoming the thermodynamic reaction barriers. The heating effect can influence the crystal packing of the NCs by providing the activation energy of transition which results in crystallographic phase transition.[63] Another important physical parameter is the pressure to change the properties of the pristine perovskite NCs. Pressure can effectively change the crystal structures, which alters the physicochemical properties by changing the bond lengths and bond angles of the inorganic framework of the perovskite NCs.[117−120] In this section, we will discuss the effect of illumination, heat, pressure, and ambient conditions on the postsynthesis transformation of the pristine NCs.

Liu et al. studied morphology transformation of $CsPbBr_3$ nanocubes into NWs under visible light illumination.[121] $CsPbBr_3$ nanocubes turned into defect-free NWs through assembly and fusion processes upon illumination of visible light (Figure 6a,b). To initiate the morphology evolution, a solar simulator with an irradiance of 1.7 suns (170 mW/cm^2) was used as a light source. The initial $CsPbBr_3$ nanocubes underwent anisotropic growth via oriented-attachment rather than through Ostwald ripening as observed by DuBose et al. for transformation of NPLs into larger NCs.[93] This transformation process is similar to the solvent-assisted transformation of nanocubes into NWs;[60,94] however, visible light illumination acted as an external stimulus for the transformation of $CsPbBr_3$ nanocubes into NWs. The morphology evolution process was accompanied by the transition from cubic to the orthorhombic crystallographic phase. The formation mechanism of NWs was explained by the light-induced selective desorption of surface ligands, namely, OA and OLAm, as evidenced from the Fourier transform infrared (FTIR) spectroscopy (Figure 6c). After photoexcitation, dissociated excitons diffused to the NCs surfaces and were captured by surface ligands (OLAm and OA). The ligand OLAm played an important role in the anisotropic NWs' morphology evolution. A small amount of OLAm facilitated the self-assembly of NWs, while excess OA led to large 3D crystals. The NWs showed a clear spectral red shift in the absorption and PL spectra compared to the original NCs (Figure 6d). The use of light to convert nanocubes into NWs provided an added degree of flexibility for morphology and crystal phase transformation of perovskite NCs.

Photon-driven transformation of $CsPbBr_3$ NPLs into its bulk analogue by continuous wave (CW) laser irradiation was reported by Wang et al.[122] The room-temperature synthesis enabled controlled growth of NPLs with precise monolayer thickness (i.e., $CsPbBr_3$ nanocubes, 3-monolayer $CsPbBr_3$ NPLs, and 5-monolayer $CsPbBr_3$ NPLs). The as-synthesized NPLs showed sharp excitonic absorbance peaks and narrow PL line widths with small Stokes shifts. The effect of illumination was studied by changing the intensity of the CW laser beam (λ = 325 nm). $CsPbBr_3$ NPLs film showed a stable PL with a peak centered at ∼436 nm up to hours with low beam intensity (∼ 5 mW/cm^2) illumination. However, upon increasing the excitation intensity to ∼20 mW/cm^2, the PL showed significant change with time, indicating the morphological transformation upon light exposure. Further detailed investigation of the photoinduced conversion of the film of $CsPbBr_3$ NPLs was carried out by dynamic in situ absorption and PL spectra with uninterrupted laser treatment. PL spectra showed a decrease of PL intensity at ∼436 nm with increasing time of laser excitation, and a new PL shoulder appeared at ∼466 nm, the intensity of which increased initially followed by quenching at a later stage. Another peak appeared at 484 nm, whose intensity also followed the same trend of the peak at 466 nm. Finally, a third peak appeared, which showed a continuous red shift approaching toward 521 nm. The intensity of the PL progressively raised and stabilized at 521 nm. After 90 min of illumination, three peaks (436, 466, and 484 nm) faded away and the PL spectrum was dominated by the peak at ∼521 nm. By comparing the PL spectrum of $CsPbBr_3$ NPLs and photoconverted $CsPbBr_3$, the PL peaks at 436, 466, 484, and 521 nm were assigned to 3-monolayer, 6-monolayer, 9-monolayer NPLs, and 3D bulk $CsPbBr_3$ nanocubes respectively. The absorbance peak of the $CsPbBr_3$ NPLs film at 431 nm progressively dropped, and new absorbance peaks appeared at ∼461 and ∼480 nm, whose energetic positions correspond to the band gap transitions of 6-monolayer and 9-monolayer $CsPbBr_3$ NPLs. With prolonged illumination, the absorbance peaks were red-shifted and smeared out. Finally, the absorption spectra followed that of the 3D $CsPbBr_3$ NCs. The photoinduced transformation of $CsPbBr_3$ NPLs was different from the usual photodarkening behavior. The gradual decrease of intensity (photodarkening) was observed primarily in traditional metal chalcogenide quantum dots, and the phenomenon was attributed to the formation of carrier

https://doi.org/10.1021/acsenergylett.2c00888
ACS Energy Lett. 2022, 7, 2136−2155

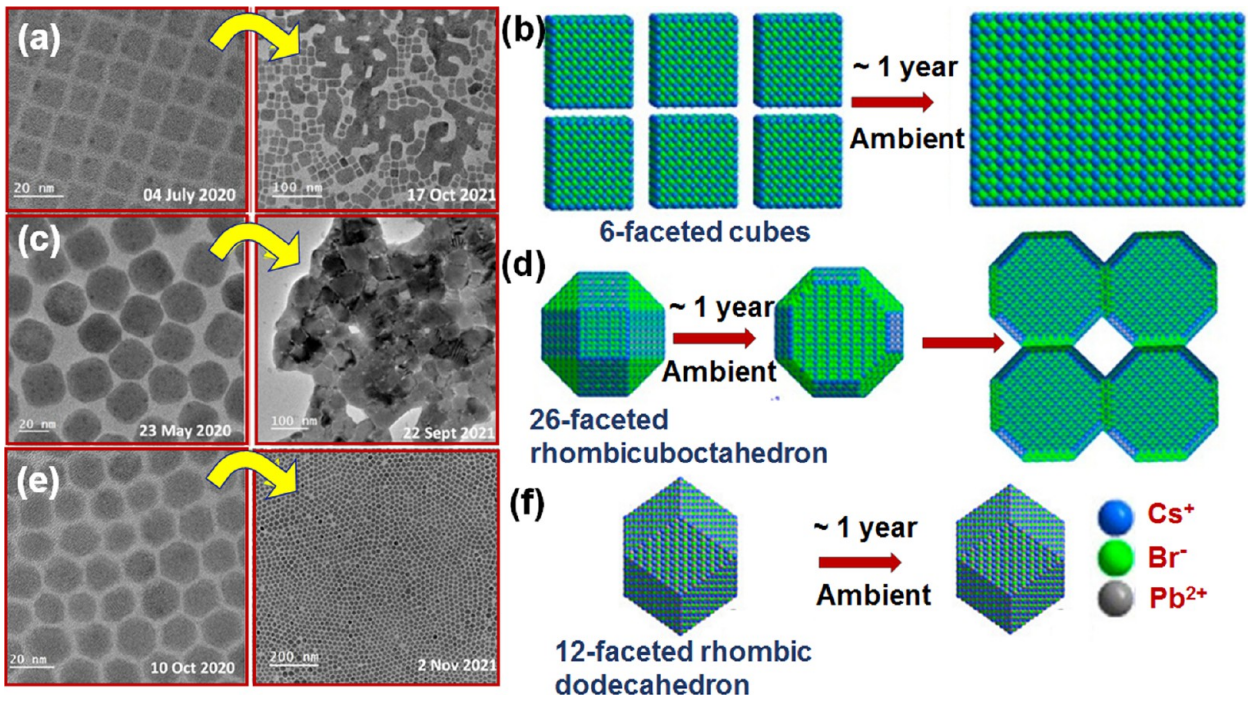

Figure 7. (a) TEM images representing morphological transformation of 6-faceted cubes into 2D sheets upon aging. (b) Atomic models showing merging of isolated cubes into 2D film with aging. Both structures are viewed along the [001] direction. (c) TEM images representing morphological transformation of 26-faceted rhombicuboctahedrons into 2D sheets upon aging. (d) Atomic models showing transformation of rhombicuboctahedron-shaped NCs to connected 2D film-type larger crystals. The viewing direction of these nanostructures is along [001]. (e) TEM images of rhombic dodecahedron NCs showing identical morphology. (f) Atomic models showing the morphology of rhombic dodecahedron NCs remain unchanged upon aging, viewed along the [100] direction. Reproduced with permission from ref 126. Copyright 2022, American Chemical Society.

trapping defects due to the photoinduced desorption of surface ligands.[123,124] However, in this case, the formation of new PL peaks at longer wavelengths from $CsPbBr_3$ NPLs film took place upon continuous laser exposure. The work demonstrated the postsynthesis multicolor luminescence change of $CsPbBr_3$ NPLs with low irradiation intensity.

The Kamat group reported reversible transformation of $Cs_2Au_2Br_6$ double-perovskite NCs under the influence of light.[125] First, $CsPbBr_3$ NCs were synthesized using the HI method, which were treated with $AuBr_3$ to obtain $Cs_2Au_2Br_6$ double-perovskite NCs along with Au nanoparticles. The metal ion exchange was reversible because $CsPbBr_3$ NCs were obtained by adding excess $PbBr_2$ to the suspension of $Cs_2Au_2Br_6$ NCs. Interestingly, photoinduced transformation of $Cs_2Au_2Br_6$ NCs into $CsPbBr_3$ NCs was shown upon visible light (λ > 400 nm; 100 mW/cm^2) exposure. $Cs_2Au_2Br_6$ NCs ejected reduced Au from the lattice to form larger Au nanoparticles, and the presence of excess Pb^{2+} ions in the suspension restored the pristine $CsPbBr_3$ composition. The $CsPbBr_3$ formed at the end of photoirradiation remained stable without undergoing additional cation exchange. The reduction of Au(I)/Au(III) to Au nanoparticles prevented further cation exchange. This work demonstrated the dynamic nature of Au within the perovskite lattice to obtain reversibility of the cubic and tetragonal crystal phases.

The surface ligands of the NCs are expected to be dynamic in solution, whereas the ligands are typically tightly bonded in solid form. Hence, the NCs should show more resistance to the polar molecules, moisture, and temperature for stability in the solid form. Pradhan and co-workers examined this aspect with NCs containing different surface ligands and surface population density using TEM after an interval of one year.[126] Green-emitting orthorhombic $CsPbBr_3$ NCs of three different shapes, namely, 6-faceted cubes, 26-faceted rhombicuboctahedrons, and 12-faceted rhombic dodecahedron shaped NCs, were considered for these aging experiments (Figure 7). The pristine NCs were observed to merge into 2D sheetlike films on the surface of the TEM grid after year-long exposure in ambient conditions (Figure 7a–d). Interestingly, the NCs retained the parent orthorhombic phase even after the morphology transformation into 2D sheets. However, such merger upon aging in the ambient conditions was observed for the 6-faceted cubes and 26-faceted rhombicuboctahedrons, while rhombic dodecahedron NCs did not show any shape transformation even after a year under similar ambient storage (Figure 7e,f). The extent of merging was more for the 26-facet rhombicuboctahedron NCs in comparison to the 6-faceted cubic NCs. These observations were directly monitored on the TEM grid; the work demonstrated postsynthesis morphology transformation of the NCs in the solid state under ambient conditions. The possible mechanism for the morphology evolution was explained by the swelling and merging of the NCs on the TEM grid surface. In the case of cubes or rhombicuboctahedrons, the surface oleylammonium ions or labile surface Cs^+ ions reacted with moisture and detached from the crystal surfaces. This opened up vacancies on the NC surfaces, and to fill these vacancies, NCs underwent self-healing to deform and connect into different shapes. On the other hand, rhombic dodecahedron NCs synthesized with tertiary *N,N*-diphenacyloleylammonium ion medium did not show any change in their shape owing to the bulky nature of the surface ligands which resisted moisture interference. These

https://doi.org/10.1021/acsenergylett.2c00888
ACS Energy Lett. 2022, 7, 2136−2155

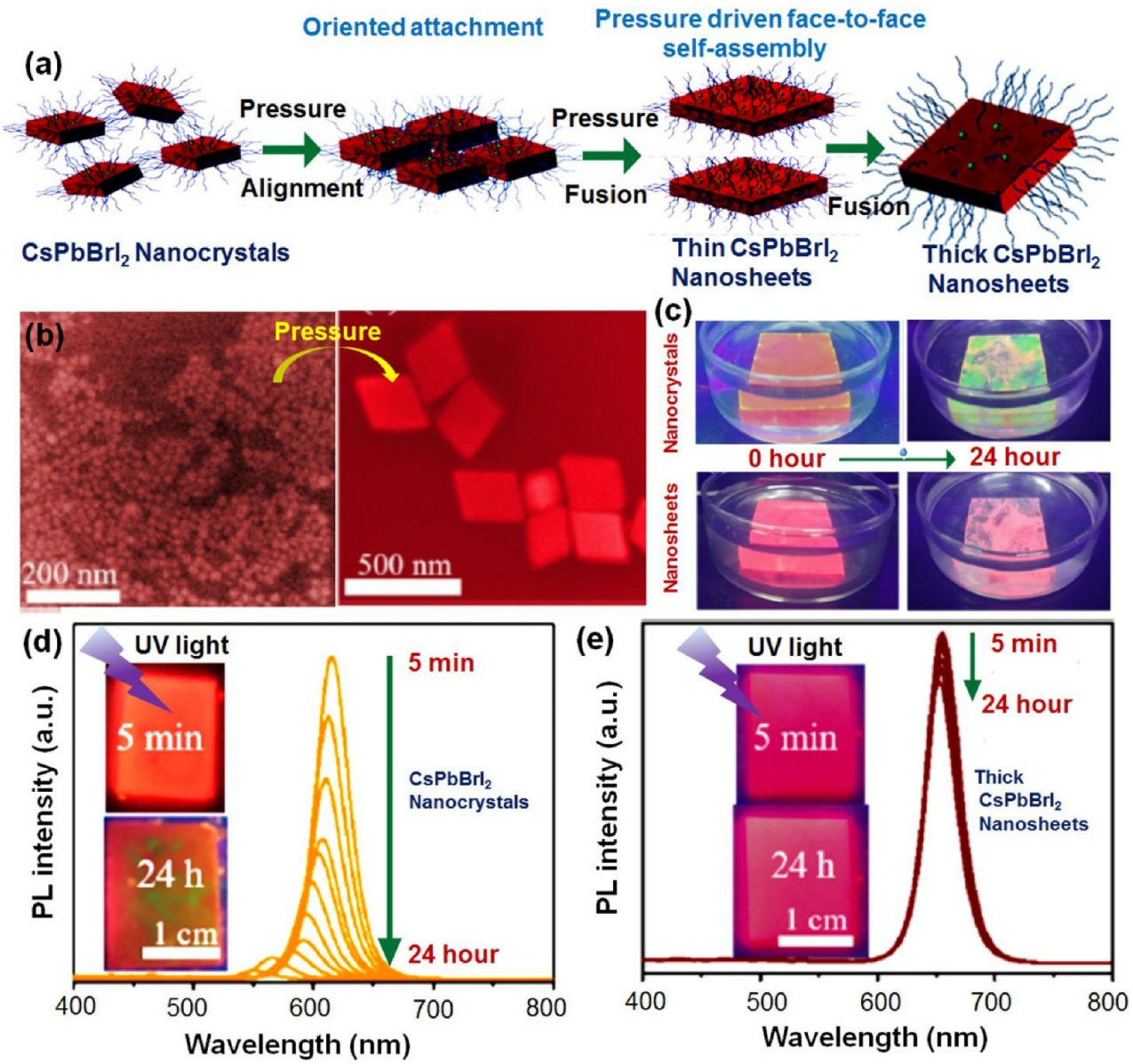

Figure 8. (a) Schematic representation of pressure-driven postsynthesis transformation of $CsPbBr_3$ NCs into $CsPbBr_3$ NSs. (b) SEM images of the NCs before and after the transformation. (c) Stability of the pristine NCs and transformed NSs upon immersion in water. (d) PL spectra of pristine NCs showing disappearance of the PL intensity upon 24 h of UV light illumination. (e) PL spectra of the thick NSs at the same condition showing retention of 85% of the original intensity. Reproduced with permission from ref 128. Copyright 2020, American Chemical Society.

results showed the role of the surface ligands for the phase and shape stability of these NCs, even in the solid form. This work also provided possible direction for forming layered single-crystalline NCs.

Huang et al. reported the morphology evolution of the $CsPbBr_3$ NCs by varying physical parameters such as illumination, moisture, oxygen, and temperature.[127] After the synthesis of $CsPbBr_3$ NCs, the morphology transformation was examined in both solution and thin film. To understand the effect of illumination on the NC morphology, 450 nm LED illumination was used. The dispersion of $CsPbBr_3$ NCs in toluene showed a PL peak at 514 nm with a full width at half-maximum of 19 nm. A red shift of the PL peak position was observed upon increasing illumination time. Subsequently, the PL intensity apparently reduced to 31.3% after 1 h of illumination and to 32.8% after 2 h of illumination. TEM images of the pristine $CsPbBr_3$ NCs revealed monodispersity with the edge lengths of 5−10 nm. However, the TEM image of the 2 h illuminated $CsPbBr_3$ NCs showed aggregate growth to larger crystals of the size range of 26−50 nm. These authors also studied the effect of humidity and oxygen. The thin film of the $CsPbBr_3$ NCs sandwiched in two quartz coverslips and the uncovered $CsPbBr_3$ NCs film were used for these studies. The sandwiched film underwent slower degradation compared to the uncovered film. From the effect of humidity, it was observed that the higher room humidity (80%) resulted in a larger PL reduction (95.6%) compared to PL reduction (89.4%) at room humidity (60%). When the thin film was exposed to pure oxygen, the green color quickly changed to yellow after 1 h of illumination, resulting in a low remnant PL

https://doi.org/10.1021/acsenergylett.2c00888
ACS Energy Lett. 2022, 7, 2136−2155

of 32.6%. Hence, oxygen played a crucial role in the degradation of $CsPbBr_3$ NCs, which was correlated with the formation of the large $CsPbBr_3$ crystals. This work demonstrated that the activity of luminescence upon the morphology transformation of the perovskite NCs strongly depended on the presence of oxygen and moisture.

The Gaponenko group reported the pressure-driven postsynthesis transformation of $CsPbBrI_2$ NCs into NSs (Figure 8a).[128] The $CsPbBrI_2$ NCs were prepared via the HI method and were transferred into an autoclave for pressure-driven transformation. Ligands started to desorb from the surfaces of the NCs upon applying isotropic pressure from all directions, reducing the steric repulsion. First, the spacing between the adjacent NCs decreased and the NCs spontaneously aligned and arranged themselves into 2D arrays driven by the dipole−dipole interaction. Ligand desorption exposed the NC surfaces for the lattice matching, and the subsequent oriented-attachment growth formed 2D NSs at higher pressure (Figure 8a). The transformed thick NSs were single-crystalline in nature. Scanning electron microscopy (SEM) images of the transformed NSs showed a parallelogram shape with edge lengths of 300−400 nm (Figure 8b). The HRTEM images revealed that the (110) crystal lattice planes of pristine cubic perovskite NCs remained the same in the NSs, suggesting that the NCs coalesced together via an oriented-attachment mechanism. Addition of a small amount of OA led to the formation of rectangular structure, whereas larger nanostructures without well-defined morphology were obtained with an excess of OA. The XRD patterns of pristine NCs revealed the coexistence of the cubic and orthorhombic phases at the initial stage. The peaks corresponding to the orthorhombic phase started to disappear with pressure, and finally the transformed NSs showed the (110) crystal planes of the cubic phase. The PL peak showed a red shift and 1.4 times higher intensity for the transformed NSs compared to the pristine NCs. The water stability of both the pristine NCs and the transformed NSs was tested by immersing the spin-casted samples in water (Figure 8c). Although the PL intensity of both samples was gradually quenched upon immersion in water, the PL quenching of the thick NSs was much slower compared to that of the NCs. The enhanced water stability of the NSs was attributed to the improved crystallinity and minimized surface area in comparison to pristine NCs, which prevented water molecules from entering into the perovskite lattice. Also, the transformed NSs exhibited enhanced PL intensity and better stability compared to the pristine NCs under the illumination of UV light (Figure 8d,e). The PL intensity of pristine NCs disappeared upon 24 h of UV light illumination; however, 85% of the original PL intensity was retained by the thick NSs in the same conditions.

Palazon et al. reported chemical, structural, and morphological transformations of the $CsPbBr_3$ NCs passivated with small molecular ligands under thermal annealing.[129] First, $CsPbBr_3$ NCs were synthesized by mixing a precursor solution of $PbBr_2$ with propionic acid, butylamine, and isopropanol. The solution was then added to a mixture containing hexane, isopropanol, and cesium-propinoate to obtain $CsPbBr_3$ NCs. The resultant NCs were drop-casted to prepare a thin film, which was annealed to 400 °C starting from room temperature. Residual solvent (toluene) was evaporated without significant structural changes on the NCs at ∼100 °C. The release of propionic acid in the temperature range of 150−350 °C triggered the phase transformation from orthorhombic $CsPbBr_3$ to tetragonal $CsPb_2Br_5$ following the equation $2CsPbBr_3 \rightarrow CsPb_2Br_5 + CsBr$ (Figure S4). Beyond 350 °C, removal of strongly bound butylamine ligands reversed the transition to the original orthorhombic phase $CsPbBr_3$. The XRD pattern revealed the orthorhombic phase for the pristine NCs, and the peaks were shifted to a lower 2θ angle during annealing because of the thermal expansion of lattices. XRD peaks corresponding to the tetragonal $CsPb_2Br_5$ phase appeared in the temperature range of 150−350 °C; however, these peaks fully disappeared above 400 °C. A photodetector device was fabricated by drop-casting a film on top of interdigitated gold electrodes on a SiO_2 substrate, and the effect of thermal annealing on the photocurrent was examined (Figure S4).

Postsynthesis transformation of the perovskite NCs changes both the structural and electronic properties of the pristine NCs. Energy-related device applications using the modified properties of the transformed perovskite NCs need to be explored.

Paul et al. reported the solid-state temperature-driven morphology evolution of the ligand-free cesium antimony chloride perovskite ($Cs_3Sb_2Cl_9$) NCs (Figure S5a).[63] Ligand-free $Cs_3Sb_2Cl_9$ perovskite NCs with hexagonal shape were prepared using a reprecipitation method at room temperature. For the synthesis of hexagonal NCs, $SbCl_3$, and CsCl were dissolved in DMF. Then 0.5 mL of this precursor solution was transferred into 5 mL of isopropanol with vigorous stirring. Because of the ionic nature of the reaction, immediate formation of NCs was observed upon mixing with isopropanol. The dried powder of hexagonal NCs was heated from 25 to 250 °C under vacuum. The temperature-dependent XRD measurements indicated a phase transition of the hexagonal shape NCs from trigonal to orthorhombic phase with increase in the temperature (Figure S5c). The phase transition process was completed at 250 °C, which was also associated with the morphology transformation of the NCs. The hexagonal shape of the NCs turned into 2D plates through solid-state reaction (Figure S5b). AFM images revealed that the height of both the hexagonal NCs and 2D plates remained the same, which indicated that transformation of the unit cells led to the reconstruction of the edges of the 2D hexagonal NCs to yield 2D plates. Both the hexagonal NCs and plates were ligand-free; hence, this postsynthesis morphology transformation was not associated with the surface ligand detachment, but rather demonstrated reconstruction of NC surfaces in the solid state via crystallographic phase transition. The above examples demonstrated the influence of heat for the postsynthesis transformation of the perovskite NCs.

In summary, to date, a variety of synthesis procedures have been established for obtaining perovskite NCs. HI and LARP processes have their own merits and demerits. However, the size and shape of the NCs were controlled using these routes during the synthesis. The postsynthetic approach provides a fruitful alternative to transform the morphologies and crystallographic phases of the as-synthesized perovskite NCs. This Focus Review covered various aspects of postsynthesis treatments and postsynthesis morphology transformation of

https://doi.org/10.1021/acsenergylett.2c00888
ACS Energy Lett. 2022, 7, 2136−2155

perovskite NCs. The dynamic nature of the coordination between the perovskite NC surface and the ligands emerged as the key factor for postsynthesis transformation. Although the postsynthetic approach introduces opportunities to change the morphologies and properties of the as-synthesized perovskite NCs, there are several open issues that require attention. It is important to understand the growth kinetics, assembly mechanisms, and surface ligand chemistry during the postsynthesis transformation process. A deeper understanding of the surface chemistry of NCs in terms of the ligand binding to the surface and the dynamics during the transformation process has not yet been realized. Furthermore, the influence of the surface termination of the NCs during the transformation requires deeper study. The change in the surface energy of NCs depending on the surface termination and the mechanism of ligand adsorption/desorption during the morphology evolution have to be elucidated. Although the postsynthetic treatments allowed transformation of the pristine morphology and crystal phase of the NCs, control over the resultant shape of the NCs remains a challenge. Preparation of complex nanostructures of the as-synthesized NCs through postsynthesis treatment is yet to be achieved. The transformation of 0D to 3D phases or vice versa by coupling or decoupling the Ruddlesden–Popper phases using postsynthesis treatments would be an interesting approach to control the dimensionality of the NCs. Achieving the ordered assemblies of the perovskite NCs using the postsynthesis routes by tuning the interparticle interactions would also be an interesting approach. From the viewpoint of applications of pristine perovskite NCs, several studies have been reported on solar cells, LEDs, photocatalysis, photodetectors, and sensors. Postsynthesis transformation of the perovskite NCs changes both the structural and electronic properties of the pristine NCs. Furthermore, light–matter interaction can also have a significant impact on the structural and optical properties of the transformed perovskite NCs. The transformed NCs often remain stable in the ambient conditions compared to the pristine NCs, a feature beneficial for device fabrication. The excitons are confined within the inorganic layer of the pristine perovskite NCs because of the reduced dimensionality affecting the charge carrier mobility and electrical conductivity. Moreover, the density of states in pristine perovskite NCs is less compared to that of larger counterparts. These drawbacks may be avoided in the transformed NCs owing to the larger dimension for improved optoelectronic applications, particularly photovoltaic, photodetector, LED, and photocatalytic applications. However, the literature showing the potential applications using the modified structural and electronic properties of the transformed NCs is limited. Some available literature contributions showed that the transformed NCs can be used for functional device fabrication (see Figures S3, S4, and S6–S8). The impressive physical properties of the transformed NCs have to be leveraged toward energy-related applications. We have only begun to understand the realm of possibilities that can be offered by postsynthesis transformation with the aim of improving and optimizing the final structures and properties of the NCs.

A deeper understanding of the surface chemistry of NCs in terms of the ligand binding to the surface and the dynamics during the transformation process has not yet been realized. Furthermore, the influence of the surface termination of the NCs during the transformation requires deeper study.

■ ASSOCIATED CONTENT

Supporting Information

The Supporting Information is available free of charge at https://pubs.acs.org/doi/10.1021/acsenergylett.2c00888.

Transformation of Cs_4PbBr_6 nanocrystals, $CsPbBr_3$ nanocrystals, phase transition of $CsPbBr_3$ nanocrystals, photodetector device fabrication, temperature-driven solid-state morphology transformation of $Cs_3Sb_2Cl_9$ nanocrystals, and light-emitting diode device fabrication using the transformed $CsPbBr_3$ nanobelts (PDF)

■ AUTHOR INFORMATION

Corresponding Author

Somobrata Acharya − *School of Applied and Interdisciplinary Sciences and Technical Research Centre, Indian Association for the Cultivation of Science, Kolkata 700032, India;* orcid.org/0000-0001-5100-5184; Email: camsa2@iacs.res.in

Author

Susmita Paul − *School of Applied and Interdisciplinary Sciences, Indian Association for the Cultivation of Science, Kolkata 700032, India*

Complete contact information is available at: https://pubs.acs.org/10.1021/acsenergylett.2c00888

Funding

SERB, India grant #CRG/2019/003907 and SERB-STAR grant #STR/2020/000053.

Notes

The authors declare no competing financial interest.

Biographies

Susmita Paul completed her M.Sc. (Chemistry) at IIT Guwahati in 2016. She joined the Ph.D. program in the School of Applied and Interdisciplinary Sciences at Indian Association for the Cultivation of Science in 2016. Presently, she is pursuing research on the structure–property evolution of perovskite nanomaterials.

Somobrata Acharya received his Ph.D. degree from Indian Association for the Cultivation of Science (IACS) in 2003. He was a postdoctoral research fellow at Ben Gurion University, Israel and ICYS fellow, National Institute for Materials Science, Japan. He is currently a Professor in the School of Applied and Interdisciplinary Sciences at IACS. http://iacs.res.in/faculty-profile.html?id=96

■ ACKNOWLEDGMENTS

We acknowledge Science and Engineering Research Board (SERB) Grant CRG/2019/003907 and SERB-STAR Grant STR/2020/000053 for financial support.

■ REFERENCES

(1) Akkerman, Q. A.; Manna, L. What Defines a Halide Perovskite? *ACS Energy Lett.* **2020**, *5*, 604–610.

(2) Mir, W. J.; Mahor, Y.; Lohar, A.; Jagadeeswararao, M.; Das, S.; Mahamuni, S.; Nag, A. Postsynthesis Doping of Mn and Yb into $CsPbX_3$ (X = Cl, Br, or I) Perovskite Nanocrystals for Down-conversion Emission. *Chem. Mater.* **2018**, *30*, 8170−8178.
(3) Brennan, M. C.; Zinna, J.; Kuno, M. Existence of a Size-Dependent Stokes Shift in $CsPbBr_3$ Perovskite Nanocrystals. *ACS Energy Lett.* **2017**, *2*, 1487−1488.
(4) Ravi, V. K.; Saikia, S.; Yadav, S.; Nawale, V. V.; Nag, A. $CsPbBr_3$/ZnS Core/Shell Type Nanocrystals for Enhancing Luminescence Lifetime and Water Stability. *ACS Energy Lett.* **2020**, *5*, 1794−1796.
(5) Di Stasio, F.; Christodoulou, S.; Huo, N.; Konstantatos, G. Near-Unity Photoluminescence Quantum Yield in $CsPbBr_3$ Nano-crystal Solid-State Films via Postsynthesis Treatment with Lead Bromide. *Chem. Mater.* **2017**, *29*, 7663−7667.
(6) Pradhan, N. Tips and Twists in Making High Photoluminescence Quantum Yield Perovskite Nanocrystals. *ACS Energy Lett.* **2019**, *4*, 1634−1638.
(7) Protesescu, L.; Yakunin, S.; Bodnarchuk, M. I.; Krieg, F.; Caputo, R.; Hendon, C. H.; Yang, R. X.; Walsh, A.; Kovalenko, M. V. Nanocrystals of Cesium Lead Halide Perovskites ($CsPbX_3$, X = Cl, Br, and I): Novel Optoelectronic Materials Showing Bright Emission with Wide Color Gamut. *Nano Lett.* **2015**, *15*, 3692−3696.
(8) Kim, J. Y.; Lee, J.-W.; Jung, H. S.; Shin, H.; Park, N.-G. High Efficiency Perovskite Solar Cells. *Chem. Rev.* **2020**, *120*, 7867−7918.
(9) Lin, R.; Xu, J.; Wei, M.; et al. All-Perovskite Tandem Solar Cells with Improved Grain Surface Passivation. *Nature* **2022**, *603*, 73−78.
(10) Kamat, P. V. Hybrid Perovskites for Multijunction Tandem Solar Cells and Solar Fuels. A Virtual Issue. *ACS Energy Lett.* **2018**, *3*, 28−29.
(11) Ravi, V. K.; Mondal, B.; Nawale, V. V.; Nag, A. Don't Let the Lead Out: New Material Chemistry Approaches for Sustainable Lead Halide Perovskite Solar Cells. *ACS Omega* **2020**, *5*, 29631−29641.
(12) Pazoki, M.; Jacobsson, T. J.; Kullgren, J.; Johansson, E. M. J.; Hagfeldt, A.; Boschloo, G.; Edvinsson, T. Photoinduced Stark Effects and Mechanism of Ion Displacement in Perovskite Solar Cell Materials. *ACS Nano* **2017**, *11*, 2823−2834.
(13) Zhao, H.; Zhou, Y.; Benetti, D.; Ma, D.; Rosei, F. Perovskite Quantum Dots Integrated in Large-Area Luminescent Solar Concentrators. *Nano Energy* **2017**, *37*, 214−223.
(14) Dursun, I.; Shen, C.; Parida, M. R.; Pan, J.; Sarmah, S. P.; Priante, D.; Alyami, N.; Liu, J.; Saidaminov, M. I.; Alias, M. S.; Abdelhady, A. L.; Ng, T. K.; Mohammed, O. F.; Ooi, B. S.; Bakr, O. M. Perovskite Nanocrystals as a Color Converter for Visible Light Communication. *ACS Photonics* **2016**, *3*, 1150−1156.
(15) Pacchioni, G. Highly Efficient Perovskite LEDs. *Nat. Rev. Mater.* **2021**, *6*, 108.
(16) Zhang, K.; Zhu, N.; Zhang, M.; Wang, L.; Xing, J. Opportunities and Challenges in Perovskite LED Commercialization. *J. Mater. Chem. C* **2021**, *9*, 3795−3799.
(17) Shynkarenko, Y.; Bodnarchuk, M. I.; Bernasconi, C.; Berezovska, Y.; Verteletskyi, V.; Ochsenbein, S. T.; Kovalenko, M. V. Direct Synthesis of Quaternary Alkylammonium Capped Perovskite Nanocrystals for Efficient Blue and Green Light-Emitting Diodes. *ACS Energy Lett.* **2019**, *4*, 2703−2711.
(18) Pang, P.; Jin, G.; Liang, C.; Wang, B.; Xiang, W.; Zhang, D.; Xu, J.; Hong, W.; Xiao, Z.; Wang, L.; Xing, G.; Chen, J.; Ma, D. Rearranging Low-Dimensional Phase Distribution of Quasi-2D Perovskites for Efficient Sky-Blue Perovskite Light-Emitting Diodes. *ACS Nano* **2020**, *14*, 11420−11430.
(19) Kumar, G. S.; Pradhan, B.; Kamilya, T.; Acharya, S. Enhancing Performances of Hybrid Perovskite Light Emitting Diodes with Thickness Controlled PMMA Interlayer. *Bull. Chem. Soc. Jpn.* **2018**, *91*, 1241−1248.
(20) Harwell, J.; Burch, J.; Fikouras, A.; Gather, M. C.; Di Falco, A.; Samuel, I. D. W. Patterning Multicolor Hybrid Perovskite Films via Top-Down Lithography. *ACS Nano* **2019**, *13*, 3823−3829.
(21) Kumar, G. S.; Sarkar, P. K.; Pradhan, B.; Hossain, M.; Rao, K. D. M.; Acharya, S. Large-Area Transparent Flexible Guanidinium Incorporated $MAPbI_3$ Microstructures for High-Performance Photodetectors with Enhanced Stability. *Nanoscale Horiz.* **2020**, *5*, 696−704.
(22) Jing, H.; Peng, R.; Ma, R.-M.; He, J.; Zhou, Y.; Yang, Z.; Li, C.-Y.; Liu, Y.; Guo, X.; Zhu, Y.; Wang, Di; Su, J.; Sun, C.; Bao, W.; Wang, M. Flexible Ultrathin Single-Crystalline Perovskite Photodetector. *Nano Lett.* **2020**, *20*, 7144−7151.
(23) Rao, K. D. M.; Hossain, M.; Umesh; Roy, A.; Ghosh, A.; Kumar, G. S.; Moitra, P.; Kamilya, T.; Acharya, S.; Bhattacharya, S. Transparent, Flexible $MAPbI_3$ Perovskite Microwire Arrays Passivated with Ultra-Hydrophobic Supramolecular Self-Assembly for Stable and High-Performance Photodetectors. *Nanoscale* **2020**, *12*, 11986.
(24) Schanze, K. S.; Kamat, P. V.; Yang, P.; Bisquert, J. Progress in Perovskite Photocatalysis. *ACS Energy Lett.* **2020**, *5*, 2602−2604.
(25) Seth, S.; Samanta, A. A Facile Methodology for Engineering the Morphology of $CsPbX_3$ Perovskite Nanocrystals under Ambient Condition. *Sci. Rep.* **2016**, *6*, 37693.
(26) Wang, A.; Yan, X.; Zhang, M.; Sun, S.; Yang, M.; Shen, W.; Pan, X.; Wang, P.; Deng, Z. Controlled Synthesis of Lead-Free and Stable Perovskite Derivative Cs_2SnI_6 Nanocrystals via a Facile Hot-Injection Process. *Chem. Mater.* **2016**, *28*, 8132−8140.
(27) Wang, S.; Amin, A. A. Y.; Wu, L.; Cao, M.; Zhang, Q.; Ameri, T. Perovskite Nanocrystals: Synthesis, Stability, and Optoelectronic Applications. *Small Struct.* **2021**, *2*, 2000124.
(28) Du, X.; Wu, G.; Cheng, J.; Dang, H.; Ma, K.; Zhang, Y.-W.; Tan, P.-F.; Chen, S. High-Quality $CsPbBr_3$ Perovskite Nanocrystals for Quantum Dot Light-Emitting Diodes. *RSC Adv.* **2017**, *7*, 10391−10396.
(29) Ashley, M. J.; O'Brien, M. N.; Hedderick, K. R.; Mason, J. A.; Ross, M. B.; Mirkin, C. A. Templated Synthesis of Uniform Perovskite Nanowire Arrays. *J. Am. Chem. Soc.* **2016**, *138*, 10096−10099.
(30) Ghosh, J.; Ghosh, R.; Giri, P. K. Mesoporous Si Nanowire Templated Controlled Fabrication of Organometal Halide Perovskite Nanoparticles with High Photo-Luminescence Quantum Yield for Light-Emitting Applications. *ACS Appl. Nano Mater.* **2018**, *1*, 1551−1562.
(31) Pradhan, B.; Kumar, G. S.; Sain, S.; Dalui, A.; Ghorai, U. K.; Pradhan, S. K.; Acharya, S. Size Tunable Cesium Antimony Chloride Perovskite Nanowires and Nanorods. *Chem. Mater.* **2018**, *30*, 2135−2142.
(32) Mehetor, S. K.; Ghosh, H.; Pradhan, N. Blue-Emitting $CsPbBr_3$ Perovskite Quantum Rods and Their Wide-Area 2D Self-Assembly. *ACS Energy Lett.* **2019**, *4*, 1437−1442.
(33) Tong, J.; Wu, J.; Shen, W.; Zhang, Y.; Liu, Y.; Zhang, T.; Nie, S.; Deng, Z. Direct Hot-Injection Synthesis of Lead Halide Perovskite Nanocubes in Acrylic Monomers for Ultrastable and Bright Nanocrystal−Polymer Composite Films. *ACS Appl. Mater. Interfaces* **2019**, *11*, 9317−9325.
(34) Pradhan, J.; Moitra, P.; Umesh; Das, B.; Mondal, P.; Kumar, G. S.; Ghorai, U. K.; Acharya, S.; Bhattacharya, S. Encapsulation of $CsPbBr_3$ Nanocrystals by a Tripodal Amine Markedly Improves Photoluminescence and Stability Concomitantly via Anion Defect Elimination. *Chem. Mater.* **2020**, *32*, 7159−7171.
(35) Huang, H.; Li, Y.; Tong, Y.; Yao, E.-P.; Feil, M. W.; Richter, A. F.; Döblinger, M.; Rogach, A. L.; Feldmann, J.; Polavarapu, L. Spontaneous Crystallization of Perovskite Nanocrystals in Nonpolar Organic Solvents: A Versatile Approach for their Shape-Controlled Synthesis. *Angew. Chem., Int. Ed.* **2019**, *58*, 16558−16562.
(36) Malgras, V.; Tominaka, S.; Ryan, J. W.; Henzie, J.; Takei, T.; Ohara, K.; Yamauchi, Y. Observation of Quantum Confinement in Monodisperse Methylammonium Lead Halide Perovskite Nanocrystals Embedded in Mesoporous Silica. *J. Am. Chem. Soc.* **2016**, *138*, 13874−13881.
(37) Feng, J.; Yan, X.; Liu, Y.; Gao, H.; Wu, Y.; Su, B.; Jiang, L. Crystallographically Aligned Perovskite Structures for High-Performance Polarization-Sensitive Photodetectors. *Adv. Mater.* **2017**, *29*, 1605993.
(38) Bodnarchuk, M. I.; Boehme, S. C.; ten Brinck, S.; Bernasconi, C.; Shynkarenko, Y.; Krieg, F.; Widmer, R.; Aeschlimann, B.;

Günther, D.; Kovalenko, M. V.; Infante, I. Rationalizing and Controlling the Surface Structure and Electronic Passivation of Cesium Lead Halide Nanocrystals. *ACS Energy Lett.* **2019**, *4*, 63−74.
(39) Kazes, M.; Udayabhaskararao, T.; Dey, S.; Oron, D. Effect of Surface Ligands in Perovskite Nanocrystals: Extending in and Reaching out. *Acc. Chem. Res.* **2021**, *54*, 1409−1418.
(40) Bera, S.; Shyamal, S.; Pradhan, N. Chemically Spiraling $CsPbBr_3$ Perovskite Nanorods. *J. Am. Chem. Soc.* **2021**, *143*, 14895−14906.
(41) Zheng, X.; Hou, Y.; Sun, H.-T.; Mohammed, O. F.; Sargent, E. H.; Bakr, O. M. Reducing Defects in Halide Perovskite Nanocrystals for Light-Emitting Applications. *J. Phys. Chem. Lett.* **2019**, *10*, 2629−2640.
(42) DuBose, J. T.; Kamat, P. V. Surface Chemistry Matters. How Ligands Influence Excited State Interactions between $CsPbBr_3$ and Methyl Viologen. *J. Phys. Chem. C* **2020**, *124*, 12990−12998.
(43) Patra, A.; Bera, S.; Nasipuri, D.; Dutta, S. K.; Pradhan, N. Tuning Facets and Controlling Monodispersity in Organic−Inorganic Hybrid Perovskite $FAPbBr_3$ Nanocrystals. *ACS Energy Lett.* **2021**, *6*, 2682−2689.
(44) De Roo, J.; Ibáñez, M.; Geiregat, P.; Nedelcu, G.; Walravens, W.; Maes, J.; Martins, J. C.; Driessche, I. V.; Kovalenko, M. V.; Hens, Z. Highly Dynamic Ligand Binding and Light Absorption Coefficient of Cesium Lead Bromide Perovskite Nanocrystals. *ACS Nano* **2016**, *10*, 2071−2081.
(45) Bai, Y.; Hao, M.; Ding, S.; Chen, P.; Wang, L. Surface Chemistry Engineering of Perovskite Quantum Dots: Strategies, Applications, and Perspectives. *Adv. Mater.* **2022**, *34*, 2105958.
(46) Dutta, A.; Behera, R. K.; Pradhan, N. Solvent Polarity: How Does This Influence the Precursor Activation, Reaction Rate, Crystal Growth, and Doping in Perovskite Nanocrystals? *ACS Energy Lett.* **2019**, *4*, 926−932.
(47) Akkerman, Q. A.; Rainò, G.; Kovalenko, M. V.; Manna, L. Genesis, Challenges and Opportunities for Colloidal Lead Halide Perovskite Nanocrystals. *Nat. Mater.* **2018**, *17*, 394−405.
(48) Haydous, F.; Gardner, J. M.; Cappel, U. B. The Impact of Ligands on the Synthesis and Application of Metal Halide Perovskite Nanocrystals. *J. Mater. Chem. A* **2021**, *9*, 23419−23443.
(49) Almeida, G.; Goldoni, L.; Akkerman, Q.; Dang, Z.; Khan, A. H.; Marras, S.; Moreels, I.; Manna, L. Role of Acid−Base Equilibria in the Size, Shape, and Phase Control of Cesium Lead Bromide Nanocrystals. *ACS Nano* **2018**, *12*, 1704−1711.
(50) Smock, S. R.; Williams, T. J.; Brutchey, R. L. Quantifying the Thermodynamics of Ligand Binding to $CsPbBr_3$ Quantum Dots. *Angew. Chem., Int. Ed.* **2018**, *57*, 11711−11715.
(51) Pradhan, N. Alkylammonium Halides for Facet Reconstruction and Shape Modulation in Lead Halide Perovskite Nanocrystals. *Acc. Chem. Res.* **2021**, *54*, 1200−1208.
(52) Udayabhaskararao, T.; Houben, L.; Cohen, H.; Menahem, M.; Pinkas, I.; Avram, L.; Wolf, T.; Teitelboim, A.; Leskes, M.; Yaffe, O.; Oron, D.; Kazes, M. A Mechanistic Study of Phase Transformation in Perovskite Nanocrystals Driven by Ligand Passivation. *Chem. Mater.* **2018**, *30*, 84−93.
(53) Ruan, L.; Shen, W.; Wang, A.; Xiang, A.; Deng, Z. Alkyl-Thiol Ligand-Induced Shape and Crystalline Phase-Controlled Synthesis of Stable Perovskite Related $CsPb_2Br_5$ Nanocrystals at Room Temperature. *J. Phys. Chem. Lett.* **2017**, *8*, 3853−3860.
(54) Sichert, J. A.; Tong, Y.; Mutz, N.; Vollmer, M.; Fischer, S.; Milowska, K. Z.; Cortadella, R. G.; Nickel, B.; Cardenas-Daw, C.; Stolarczyk, J. K.; Urban, A. S.; Feldmann, J. Quantum Size Effect in Organometal Halide Perovskite Nanoplatelets. *Nano Lett.* **2015**, *15*, 6521−6527.
(55) Butkus, J.; Vashishtha, P.; Chen, K.; Gallaher, J. K.; Prasad, S. K. K.; Metin, D. Z.; Laufersky, G.; Gaston, N.; Halpert, J. E.; Hodgkiss, J. M. The Evolution of Quantum Confinement in $CsPbBr_3$ Perovskite Nanocrystals. *Chem. Mater.* **2017**, *29*, 3644−3652.
(56) Dutta, S. K.; Bera, S.; Behera, R. K.; Hudait, B.; Pradhan, N. Cs-Lattice Extension and Expansion for Inducing Secondary Growth of $CsPbBr_3$ Perovskite Nanocrystals. *ACS Nano* **2021**, *15*, 16183−16193.
(57) Shamsi, J.; Dang, Z.; Ijaz, P.; Abdelhady, A. L.; Bertoni, G.; Moreels, I.; Manna, L. Colloidal CsX (X = Cl, Br, I) Nanocrystals and Their Transformation to $CsPbX_3$ Nanocrystals by Cation Exchange. *Chem. Mater.* **2018**, *30*, 79−83.
(58) Bao, X.; Li, M.; Zhao, J.; Xia, Z. The Postsynthetic Anion Exchange of $Cspbi_3$ Nanocrystals for Photoluminescence Tuning and Enhanced Quantum Efficiency. *J. Mater. Chem. C* **2020**, *8*, 12302.
(59) Ghorai, A.; Midya, A.; Ray, S. K. Surfactant-Induced Anion Exchange and Morphological Evolution for Composition-Controlled Caesium Lead Halide Perovskites with Tunable Optical Properties. *ACS Omega* **2019**, *4*, 12948−12954.
(60) Sun, J.-K.; Huang, S.; Liu, X.-Z.; et al. Polar Solvent Induced Lattice Distortion of Cubic $CsPbI_3$ Nanocubes and Hierarchical Self-Assembly into Orthorhombic Single-Crystalline Nanowires. *J. Am. Chem. Soc.* **2018**, *140*, 11705−11715.
(61) Palazon, F.; Almeida, G.; Akkerman, Q. A.; De Trizio, L.; Dang, Z.; Prato, M.; Manna, L. Changing the Dimensionality of Cesium Lead Bromide Nanocrystals by Reversible Postsynthesis Transformations with Amines. *Chem. Mater.* **2017**, *29*, 4167−4171.
(62) Akkerman, Q. A.; Park, S.; Radicchi, E.; Nunzi, F.; Mosconi, E.; De Angelis, F.; Brescia, R.; Rastogi, P.; Prato, M.; Manna, L. Nearly Monodisperse Insulator Cs_4PbX_6 (X = Cl, Br, I) Nanocrystals, Their Mixed Halide Compositions, and Their Transformation into $CsPbX_3$ Nanocrystals. *Nano Lett.* **2017**, *17*, 1924−1930.
(63) Paul, S.; Sain, S.; Kamilya, T.; Dalui, A.; Sarkar, P. K.; Acharya, S. Shape Tunable Two−Dimensional Ligand−Free Cesium Antimony Chloride Perovskites. *Mater. Today Chem.* **2022**, *23*, 100641.
(64) Shamsi, J.; Urban, A. S.; Imran, M.; De Trizio, L.; Manna, L. Metal Halide Perovskite Nanocrystals: Synthesis, Post-Synthesis Modifications, and Their Optical Properties. *Chem. Rev.* **2019**, *119*, 3296−3348.
(65) Liu, M.; Matuhina, A.; Zhang, H.; Vivo, P. Advances in the Stability of Halide Perovskite Nanocrystals. *Materials* **2019**, *12*, 3733.
(66) Thumu, U.; Piotrowski, M.; Owens-Baird, B.; Kolen'ko, Y. V. Zero-Dimensional Cesium Lead Halide Perovskites: Phase Transformations, Hybrid Structures, and Applications. *J. Solid State Chem.* **2019**, *271*, 361−377.
(67) Toso, S.; Baranov, D.; Manna, L. Metamorphoses of Cesium Lead Halide Nanocrystals. *Acc. Chem. Res.* **2021**, *54*, 498−508.
(68) Saruyama, M.; Sato, R.; Teranishi, T. Transformations of Ionic Nanocrystals via Full and Partial Ion Exchange Reactions. *Acc. Chem. Res.* **2021**, *54*, 765−775.
(69) Huang, H.; Bodnarchuk, M. I.; Kershaw, S. V.; Kovalenko, M. V.; Rogach, A. L. Lead Halide Perovskite Nanocrystals in the Research Spotlight: Stability and Defect Tolerance. *ACS Energy Lett.* **2017**, *2*, 2071−2083.
(70) Wang, H.-C.; Lin, S.-Y.; Tang, A.-C.; Singh, B. P.; Tong, H.-C.; Chen, C.-Y.; Lee, Y.-C.; Tsai, T.-L.; Liu, R.-S. Mesoporous Silica Particles Integrated with All-Inorganic $CsPbBr_3$ Perovskite Quantum-Dot Nanocomposites (MP-PQDs) with High Stability and Wide Color Gamut Used for Backlight Display. *Angew. Chem., Int. Ed.* **2016**, *55*, 7924−7929.
(71) Zhuo, S.; Zhang, J.; Shi, Y.; Huang, Y.; Zhang, B. Self-Template-Directed Synthesis of Porous Perovskite Nanowires at Room Temperature for High-Performance Visible-Light Photodetectors. *Angew. Chem., Int. Ed.* **2015**, *54*, 5693−5696.
(72) Hong, K.; Le, Q. V.; Kim, S. Y.; Jang, H. W. Low-Dimensional Halide Perovskites: Review and Issues. *J. Mater. Chem. C* **2018**, *6*, 2189−2209.
(73) Wang, H.-C.; Bao, Z.; Tsai, H.-Y.; Tang, A.-C.; Liu, R.-S. Perovskite Quantum Dots and Their Application in Light-Emitting Diodes. *Small* **2018**, *14*, 1702433.
(74) Murray, C. B.; Norris, D. J.; Bawendi, M. G. Synthesis and Characterization of Nearly Monodisperse CdE (E = Sulfur, Selenium, Tellurium) Semiconductor Nanocrystallites. *J. Am. Chem. Soc.* **1993**, *115*, 8706−8715.

https://doi.org/10.1021/acsenergylett.2c00888
ACS Energy Lett. 2022, 7, 2136−2155

(75) Yu, W. W.; Peng, X. Formation of High-Quality CdS and Other II-VI Semiconductor Nanocrystals in Noncoordinating Sol-vents: Tunable Reactivity of Monomers. *Angew. Chem., Int. Ed.* **2002**, *41*, 2368−2371.
(76) Huang, H.; Polavarapu, L.; Sichert, J. A.; Susha, A. S.; Urban, A. S.; Rogach, A. L. Colloidal Lead Halide Perovskite Nanocrystals: Synthesis, Optical Properties and Applications. *NPG Asia Mater.* **2016**, *8*, e328.
(77) Bullen, C. R.; Mulvaney, P. Nucleation and Growth Kinetics of CdSe Nanocrystals in Octadecene. *Nano Lett.* **2004**, *4*, 2303−2307.
(78) Deka, S.; Genovese, A.; Zhang, Y.; Miszta, K.; Bertoni, G.; Krahne, R.; Giannini, C.; Manna, L. Phosphine-Free Synthesis of p-Type Copper(I) Selenide Nanocrystals in Hot Coordinating Solvents. *J. Am. Chem. Soc.* **2010**, *132*, 8912−8914.
(79) Yang, B.; Chen, J.; Hong, F.; Mao, X.; Zheng, K.; Yang, S.; Li, Y.; Pullerits, T.; Deng, W.; Han, K. Lead-Free, Air-Stable All-Inorganic Cesium Bismuth Halide Perovskite Nanocrystals. *Angew. Chem., Int. Ed.* **2017**, *56*, 12471−12475.
(80) Zhang, J.; Yang, Y.; Deng, H.; Farooq, U.; Yang, X.; Khan, J.; Tang, J.; Song, H. High Quantum Yield Blue Emission from Lead-Free Inorganic Antimony Halide Perovskite Colloidal Quantum Dots. *ACS Nano* **2017**, *11*, 9294−9302.
(81) Yang, B.; Chen, J.; Yang, S.; Hong, F.; Sun, L.; Han, P.; Pullerits, T.; Deng, W.; Han, K. Lead-Free Silver-Bismuth Halide Double Perovskite Nanocrystals. *Angew. Chem., Int. Ed.* **2018**, *57*, 5359−5363.
(82) Paul, S.; Ariga, K.; Sarma, D. D.; Acharya, S. Dimension-Controlled Halide Perovkites using Templates. *Nano Today* **2021**, *39*, 101181.
(83) Liu, W.; Zhou, H.; Chen, G. Patterned Lead Halide Perovskite Crystals Fabricated by Microstructured Templates. *Cryst. Growth Des.* **2020**, *20*, 2803−2816.
(84) Dey, A.; Ye, J.; De, A.; Debroye, E.; et al. State of the Art and Prospects for Halide Perovskite Nanocrystals. *ACS Nano* **2021**, *15*, 10775−10981.
(85) Chouhan, L.; Ghimire, S.; Subrahmanyam, C.; Miyasaka, T.; Biju, V. Synthesis, Optoelectronic Properties and Applications of Halide Perovskites. *Chem. Soc. Rev.* **2020**, *49*, 2869−2885.
(86) Ahmed, G. H.; Yin, J.; Bakr, O. M.; Mohammed, O. F. Successes and Challenges of Core/Shell Lead Halide Perovskite Nanocrystals. *ACS Energy Lett.* **2021**, *6*, 1340−1357.
(87) Hills-Kimball, K.; Yang, H.; Cai, T.; Wang, J.; Chen, O. Recent Advances in Ligand Design and Engineering in Lead Halide Perovskite Nanocrystals. *Adv. Sci.* **2021**, *8*, 2100214.
(88) Toso, S.; Baranov, D.; Manna, L. Hidden in Plain Sight: The Overlooked Influence of the Cs+ Substructure on Transformations in Cesium Lead Halide Nanocrystals. *ACS Energy Lett.* **2020**, *5*, 3409−3414.
(89) Xu, Y.; Cao, M.; Huang, S. Recent Advances and Perspective on the Synthesis and Photocatalytic Application of Metal Halide Perovskite Nanocrystals. *Nano Res.* **2021**, *14*, 3773−3794.
(90) Heuer-Jungemann, A.; Feliu, N.; Bakaimi, I.; Hamaly, M.; Alkilany, A.; Chakraborty, I.; Masood, A.; Casula, M. F.; Kostopoulou, A.; Oh, E.; Susumu, K.; Stewart, M. H.; Medintz, I. L.; Stratakis, E.; Parak, W. J.; Kanaras, A. G. The Role of Ligands in the Chemical Synthesis and Applications of Inorganic Nanoparticles. *Chem. Rev.* **2019**, *119*, 4819−4880.
(91) Stelmakh, A.; Aebli, M.; Baumketner, A.; Kovalenko, M. V. On the Mechanism of Alkylammonium Ligands Binding to the Surface of $CsPbBr_3$ Nanocrystals. *Chem. Mater.* **2021**, *33*, 5962−5973.
(92) Pazoki, M.; Edvinsson, T. Metal Replacement in Perovskite Solar Cell Materials: Chemical Bonding Effects and Optoelectronic Properties. *Sustain. Energy Fuels* **2018**, *2*, 1430−1445.
(93) DuBose, J. T.; Christy, A.; Chakkamalayath, J.; Kamat, P. V. Transformation of Perovskite Nanoplatelets to Large Nanostructures Driven by Solvent Polarity. *ACS Materials Lett.* **2022**, *4*, 93−101.
(94) Pradhan, B.; Mushtaq, A.; Roy, D.; Sain, S.; Das, B.; Ghorai, U. K.; Pal, S. K.; Acharya, S. Postsynthesis Spontaneous Coalescence of Mixed-Halide Perovskite Nanocubes into Phase-Stable Single-Crystalline Uniform Luminescent Nanowires. *J. Phys. Chem. Lett.* **2019**, *10*, 1805−1812.
(95) Ghosh, S.; Manna, L. The Many "Facets" of Halide Ions in the Chemistry of Colloidal Inorganic Nanocrystals. *Chem. Rev.* **2018**, *118*, 7804−7864.
(96) Sadighian, J. C.; Wong, C. Y. Just Scratching the Surface: In Situ and Surface-Specific Characterization of Perovskite Nanocrystal Growth. *J. Phys. Chem. C* **2021**, *125*, 20772−20782.
(97) Tan, S.; Huang, T.; Yavuz, I.; et al. Surface Reconstruction of Halide Perovskites during Post-treatment. *J. Am. Chem. Soc.* **2021**, *143*, 6781−6786.
(98) Baranov, D.; Caputo, G.; Goldoni, L.; Dang, Z.; Scarfiello, R.; De Trizio, L.; Portone, A.; Fabbri, F.; Camposeo, A.; Pisignano, D.; Manna, L. Transforming Colloidal Cs_4PbBr_6 Nanocrystals with Poly(Maleic Anhydride-Alt-1-Octadecene) into Stable $CsPbBr_3$ Perovskite Emitters through Intermediate Heterostructures. *Chem. Sci.* **2020**, *11*, 3986−3995.
(99) Palazon, F.; Urso, C.; De Trizio, L.; Akkerman, Q.; Marras, S.; Locardi, F.; Nelli, I.; Ferretti, M.; Prato, M.; Manna, L. Postsynthesis Transformation of Insulating Cs_4PbBr_6 Nanocrystals into Bright Perovskite $CsPbBr_3$ through Physical and Chemical Extraction of CsBr. *ACS Energy Lett.* **2017**, *2*, 2445−2448.
(100) Zhai, W.; Lin, J.; Li, Q.; Zheng, K.; Huang, Y.; Yao, Y.; He, X.; Li, L.; Yu, C.; Liu, C.; Fang, Y.; Liu, Z.; Tang, C. Solvothermal Synthesis of Ultrathin Cesium Lead Halide Perovskite Nanoplatelets with Tunable Lateral Sizes and Their Reversible Transformation into Cs_4PbBr_6 Nanocrystals. *Chem. Mater.* **2018**, *30*, 3714−3721.
(101) Yang, H.; Cai, T.; Dube, L.; Hills-Kimball, K.; Chen, O. Synthesis of Ultrathin Perovskite Nanowires via a Postsynthetic Transformation Reaction of Zero-Dimensional Perovskite Nanocrystals. *Cryst. Growth Des.* **2021**, *21*, 1924−1930.
(102) Zhang, D.; Yu, Y.; Bekenstein, Y.; Wong, A. B.; Alivisatos, A. P.; Yang, P. Ultrathin Colloidal Cesium Lead Halide Perovskite Nanowires. *J. Am. Chem. Soc.* **2016**, *138*, 13155−13158.
(103) Jia, C.; Li, H.; Meng, X.; Li, H. $CsPbX_3/Cs_4PbX_6$ Core/Shell Perovskite Nanocrystals. *Chem. Commun.* **2018**, *54*, 6300−6303.
(104) Li, F.; Liu, Y.; Wang, H.; Zhan, Q.; Liu, Q.; Xia, Z. Postsynthetic Surface Trap Removal of $CsPbX_3$ (X = Cl, Br, or I) Quantum Dots via a ZnX_2/Hexane Solution toward an Enhanced Luminescence Quantum Yield. *Chem. Mater.* **2018**, *30*, 8546−8554.
(105) Ji, Y.; Wang, M.; Yang, Z.; Ji, S.; Qiu, H.; Dou, J.; Gaponenko, N. V. Reversible Transformation between $CsPbBr_3$ Nanowires and Nanoparticles. *Chem. Commun.* **2019**, *55*, 12809−12812.
(106) Ravi, V. K.; Scheidt, R. A.; Nag, A.; Kuno, M.; Kamat, P. V. To Exchange or Not to Exchange. Suppressing Anion Exchange in Cesium Lead Halide Perovskites with $PbSO_4$−Oleate Capping. *ACS Energy Lett.* **2018**, *3*, 1049−1055.
(107) Fanizza, E.; Cascella, F.; Altamura, D.; Giannini, C.; Panniello, A.; Triggiani, L.; Panzarea, F.; Depalo, N.; Grisorio, R.; Suranna, G. P.; Agostiano, A.; Curri, M. L.; Striccoli, M. Post-Synthesis Phase and Shape Evolution of $CsPbBr_3$ Colloidal Nanocrystals: The Role of Ligands. *Nano Res.* **2019**, *12*, 1155−1166.
(108) Zhang, D.; Eaton, S. W.; Yu, Y.; Dou, L.; Yang, P. Solution-Phase Synthesis of Cesium Lead Halide Perovskite Nanowires. *J. Am. Chem. Soc.* **2015**, *137*, 9230−9233.
(109) Balakrishnan, S. K.; Kamat, P. V. Ligand Assisted Transformation of Cubic $CsPbBr_3$ Nanocrystals into Two-Dimensional $CsPb_2Br_5$ Nanosheets. *Chem. Mater.* **2018**, *30*, 74−78.
(110) Yang, H.; Cai, T.; Liu, E.; Hills-Kimball, K.; Gao, J.; Chen, O. Synthesis and Transformation of Zero-dimensional Cs_3BiX_6 (X = Cl, Br) Perovskite-Analogue Nanocrystals. *Nano Res.* **2020**, *13*, 282−291.
(111) Yang, H.; Cai, T.; Dube, L.; Chen, O. Synthesis of Double Perovskite and Quadruple Perovskite Nanocrystals through Post-Synthetic Transformation Reactions. *Chem. Sci.* **2022**, *13*, 4874−4883.
(112) Ummadisingu, A.; Steier, L.; Seo, J.-Y.; Matsui, T.; Abate, A.; Tress, W.; Grätzel, M. The Effect of Illumination on the Formation of Metal Halide Perovskite Films. *Nature* **2017**, *545*, 208−212.

(113) Bakr, O. M.; Mohammed, O. F. Shedding Light on Film Crystallization. *Nat. Mater.* **2017**, *16*, 601−602.
(114) Kirschner, M. S.; Diroll, B. T.; Guo, P.; et al. Photoinduced, Reversible Phase Transitions in All-Inorganic Perovskite Nanocrystals. *Nat. Commun.* **2019**, *10*, 504.
(115) Xue, J.; Yang, D.; Cai, B.; Xu, X.; Wang, J.; Ma, H.; Yu, X.; Yuan, G.; Zou, Y.; Song, J.; Zeng, H. Photon-Induced Reversible Phase Transition in $CsPbBr_3$ Perovskite. *Adv. Funct. Mater.* **2019**, *29*, 1807922.
(116) Sarmah, S. P.; Burlakov, V. M.; Yengel, E.; et al. Double Charged Surface Layers in Lead Halide Perovskite Crystals. *Nano Lett.* **2017**, *17*, 2021−2027.
(117) Li, Q.; Zhang, L.; Chen, Z.; Quan, Z. Metal Halide Perovskites under Compression. *J. Mater. Chem. A* **2019**, *7*, 16089−16108.
(118) Zhang, L.; Wang, K.; Lin, Y.; Zou, B. Pressure Effects on the Electronic and Optical Properties in Low-Dimensional Metal Halide Perovskites. *J. Phys. Chem. Lett.* **2020**, *11*, 4693−4701.
(119) Jaffe, A.; Lin, Y.; Karunadasa, H. I. Halide Perovskites under Pressure: Accessing New Properties through Lattice Compression. *ACS Energy Lett.* **2017**, *2*, 1549−1555.
(120) Nagaoka, Y.; Hills-Kimball, K.; Tan, R.; Li, R.; Wang, Z.; Chen, O. Nanocube Superlattices of Cesium Lead Bromide Perovskites and Pressure-Induced Phase Transformations at Atomic and Mesoscale Levels. *Adv. Mater.* **2017**, *29*, 1606666.
(121) Liu, J.; Song, K.; Shin, Y.; et al. Light-Induced Self-Assembly of Cubic $CsPbBr_3$ Perovskite Nanocrystals into Nanowires. *Chem. Mater.* **2019**, *31*, 6642−6649.
(122) Wang, Y.; Li, X.; Sreejith, S.; Cao, F.; Wang, Z.; Stuparu, M. C.; Zeng, H.; Sun, H. Photon Driven Transformation of Cesium Lead Halide Perovskites from Few-Monolayer Nanoplatelets to Bulk Phase. *Adv. Mater.* **2016**, *28*, 10637−10643.
(123) Park, Y.; Felipe, M. J.; Advincula, R. C. Facile Patterning of Hybrid CdSe Nanoparticle Films by Photoinduced Surface Defects. *ACS Appl. Mater. Interfaces* **2011**, *3*, 4363−4369.
(124) Malak, S. T.; Jung, J.; Yoon, Y. J.; Smith, M. J.; Lin, C. H.; Lin, Z.; Tsukruk, V. V. Large-Area Multicolor Emissive Patterns of Quantum Dot−Polymer Films via Targeted Recovery of Emission Signature. *Adv. Optical Mater.* **2016**, *4*, 608−619.
(125) Chakkamalayath, J.; Hartland, G. V.; Kamat, P. V. Photo-induced Transformation of $Cs_2Au_2Br_6$ into $CsPbBr_3$ Nanocrystals. *J. Phys. Chem. Lett.* **2022**, *13*, 2921−2927.
(126) Dutta, S. K.; Bera, S.; Sen, S.; Pradhan, N. What Happens to Halide Perovskite Nanocrystals on TEM Grids upon Year-Long Ambient Storage? Surface Ligands versus Crystal Stability. *ACS Energy Lett.* **2022**, *7*, 773−777.
(127) Huang, S.; Li, Z.; Wang, B.; Zhu, N.; Zhang, C.; Kong, L.; Zhang, Q.; Shan, A.; Li, L. Morphology Evolution and Degradation of $CsPbBr_3$ Nanocrystals under Blue Light-Emitting Diode Illumination. *ACS Appl. Mater. Interfaces* **2017**, *9*, 7249−7258.
(128) Ji, Y.; Wang, M.; Yang, Z.; Qiu, H.; Kou, S.; Padhiar, M. A.; Bhatti, A. S.; Gaponenko, N. V. Pressure-Driven Transformation of $CsPbBrI_2$ Nanoparticles into Stable Nanosheets in Solution through Self-Assembly. *J. Phys. Chem. Lett.* **2020**, *11*, 9862−9868.
(129) Palazon, F.; Dogan, S.; Marras, S.; Locardi, F.; Nelli, I.; Rastogi, P.; Ferretti, M.; Prato, M.; Krahne, R.; Manna, L. From $CsPbBr_3$ Nano-Inks to Sintered $CsPbBr_3$−$CsPb_2Br_5$ Films via Thermal Annealing: Implications on Optoelectronic Properties. *J. Phys. Chem. C* **2017**, *121*, 11956−11961.

https://doi.org/10.1021/acsenergylett.2c00888
ACS Energy Lett. 2022, 7, 2136−2155